ARMY RESEARCH LABORATORY

# Analyses of Millimeter Wave Radar Low-Angle Ground-Clutter Measurements for European-Like and Desert Environments

by Ronald Wellman, Geoff Goldman,
Jerry Silvious, and David Hutchins

ARL-TR-1102 July 1996

The findings in this report are not to be construed as an official Department of the Army position unless so designated by other authorized documents.

Citation of manufacturer's or trade names does not constitute an official endorsement or approval of the use thereof.

Destroy this report when it is no longer needed. Do not return it to the originator.

# DISCLAIMER NOTICE

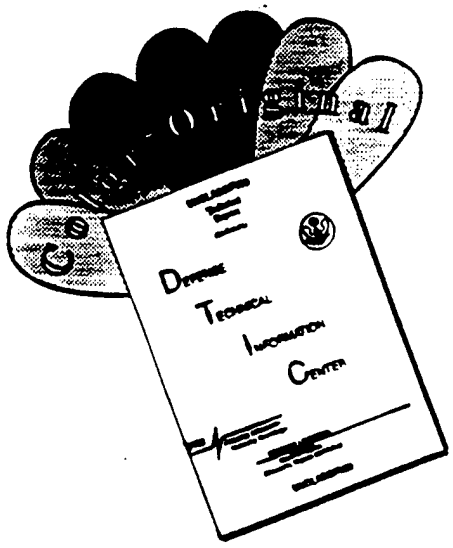


THIS DOCUMENT IS BEST QUALITY AVAILABLE. THE COPY FURNISHED TO DTIC CONTAINED A SIGNIFICANT NUMBER OF COLOR PAGES WHICH DO NOT REPRODUCE LEGIBLY ON BLACK AND WHITE MICROFICHE.

# REPORT DOCUMENTATION PAGE

*Form Approved*
*OMB No. 0704-0188*



| 1. AGENCY USE ONLY *(Leave blank)* | 2. REPORT DATE | 3. REPORT TYPE AND DATES COVERED |
|---|---|---|
| | July 1996 | Final, from September 1992 to May 1994 |

**4. TITLE AND SUBTITLE**
Analyses of Millimeter Wave Radar Low-Angle Ground-Clutter Measurements for European-Like and Desert Environments

**5. FUNDING NUMBERS**
PE: 62784A

**6. AUTHOR(S)**
Ronald Wellman, Geoff Goldman, Jerry Silvious, and David Hutchins

**7. PERFORMING ORGANIZATION NAME(S) AND ADDRESS(ES)**
U.S. Army Research Laboratory
Attn: AMSRL-SE-RM
2800 Powder Mill Road
Adelphi, MD 20783-1197

**8. PERFORMING ORGANIZATION REPORT NUMBER**
ARL-TR-1102

**9. SPONSORING/MONITORING AGENCY NAME(S) AND ADDRESS(ES)**
U.S. Army CRREL, Corps of Engineers
Hanover, NH 03755-1290

**10. SPONSORING/MONITORING AGENCY REPORT NUMBER**

**11. SUPPLEMENTARY NOTES**
AMS code: 612784.T42
ARL PR: 554L54

**12a. DISTRIBUTION/AVAILABILITY STATEMENT**
Approved for public release; distribution unlimited.

**12b. DISTRIBUTION CODE**

**13. ABSTRACT** *(Maximum 200 words)*

This report describes millimeter wave ground-based radar cross-section measurements taken to support the SWOE JT&E program over two years. RCS measurements were made on selected ground-clutter patches for one month and over another 43-day period at Camp Grayling, MI; and for 47 days at Yuma Proving Ground, AZ. Instruments collected data on meteorological conditions, solar flux, and soil moisture content.

A wide range of atmospheric conditions was observed in Grayling over the measurement periods. The conditions in Yuma over the measurement period were relatively stable. In this report, we describe the variations in the ground-based measured RCS of different clutter types over time and space for environmental conditions encountered during the three field tests. We have developed and will present an empirical model to describe these variations for the Yuma and Grayling II environments.

| 14. SUBJECT TERMS | 15. NUMBER OF PAGES |
|---|---|
| MMW, clutter, low angle, 95 GHz | 63 |
| | 16. PRICE CODE |

| 17. SECURITY CLASSIFICATION OF REPORT | 18. SECURITY CLASSIFICATION OF THIS PAGE | 19. SECURITY CLASSIFICATION OF ABSTRACT | 20. LIMITATION OF ABSTRACT |
|---|---|---|---|
| Unclassified | Unclassified | Unclassified | UL |

NSN 7540-01-280-5500

Standard Form 298 (Rev. 2-89)
Prescribed by ANSI Std. Z39-18
298-102

# Contents



# Figures

## Tables

# 1. Introduction

Sensor systems operating at about 95 GHz are being investigated for use in smart munitions designed to defeat armored vehicles [1]. These systems require specific information on the millimeter wave (MMW)* background environments that can be encountered, in order to predict their target-detection performance in a real environment. This information can be obtained from actual MMW background measurements, or from a validated MMW clutter model. The data presented in this report were taken to assist in the validation of a millimeter wave background model for the Smart Weapons Operability Enhancement (SWOE) program managed by the U.S. Army's Cold Regions Research and Engineering Laboratory. The aim of the SWOE program is to produce validated models for simulating real-world environments for both the infrared (IR) and MMW regions of the spectrum. The Army Research Laboratory (ARL) was not directly involved in the MMW modeling effort, but to support the modeling work, we developed empirical models for the 95-GHz circular polarization radar clutter data obtained over a 6- to 7-week time period at Yuma, AZ, and Grayling, MI. We discuss the radar, calibration, and measurement procedures in section 2 of this report, and the measured data in section 3. In section 4, we describe the empirical modeling procedure and results, and we present our conclusions in section 5.

*An acronym list is provided at the end of this document to assist the reader.*

# 2. Ground-Based Radar Description and Measurements

## 2.1 Description of the Radar System

The radar used for these measurements has been discussed in detail previously [2,3]. Only a brief description of the radar as configured for this test will be presented. The radar was designed for obtaining 95-GHz target- and background-signature data, with the radar located on a tower and computer-controlled from a remote ground station. Figure 1 shows the radar and the computer-controlled pedestal set up for the field test at Grayling. A video camera that is boresighted with the radar records the radar scene through a glass window at the upper-right-hand corner of the metallic cover. The radar power supply and temperature-control air conditioner are also shown in the photograph. The radar is protected from rain or snow by the tent during operation and storage. Data recording and control of the radar are performed at a ground station located in an 11-m-long semitrailer. Data from the target platform and a meteorological station may also be recorded at that location.

The basic characteristics of the ground-based radar are summarized below:

- Frequency—95.0 GHz,
- Two-coordinate amplitude-comparison monopulse,
- Polarization agile—RHCP/LHCP or V/H (selectable),
- Coherent and wide bandwidth,
- Frequency steppable—1 to 512 steps, 1-, 2-, 5-, 10-, 20-MHz stepsize,
- Peak power—45 W,
- Pulse width—100 ns,
- Pulse repetition frequency—10 kHz,
- Antenna beamwidth (one way)—0.3 to 5° (1.5° for these tests),
- Receiver IF bandwidth—30 MHz,
- Receiver noise figure—10 dB,
- Dynamic range (amplitude)—66 dB, and
- Data recording—16 channels for each pulse.

The radar is a completely polarimetric, two-coordinate, amplitude-comparison monopulse system. It is a fully coherent, dual polarization, pulsed radar that operates in a frequency-stepped mode, between 95.00 and 95.64 GHz. For the first two tests, we operated the system with 64 10-MHz steps and a transmit PRF of 10 kHz; for the second Grayling test, we used 128 5-MHz steps. The peak power of the all-solid-state transmitter is 45 W; the pulse width is 100 ns; and we swept the location of the end of

Figure 1. Ground-based 95-GHz monopulse radar at Camp Grayling, MI.

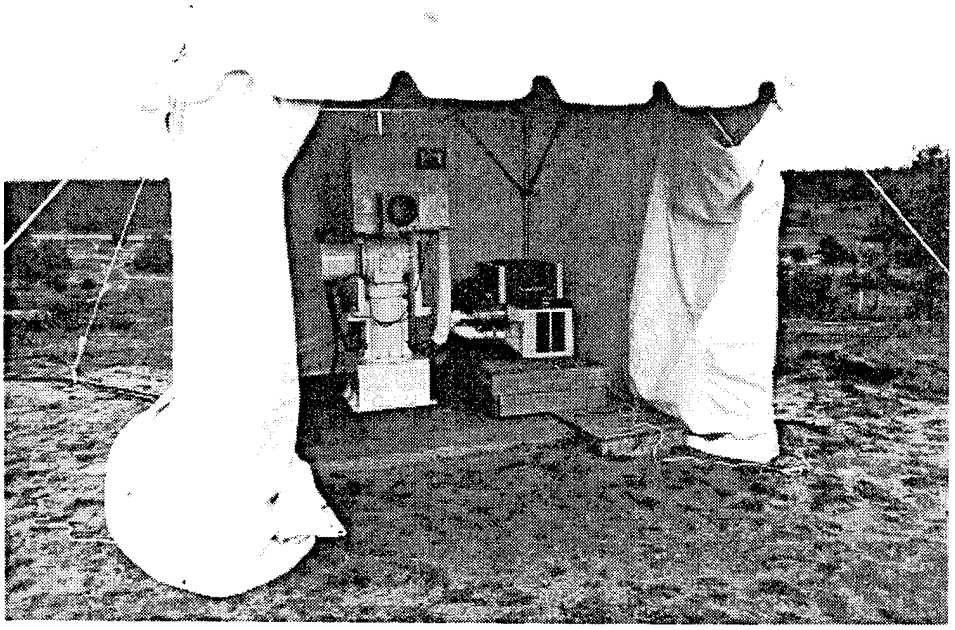

the 15-m-long range gate sequentially from 105 to 255 m. We switched the polarization from pulse-to-pulse, and obtained both linear and circular data. We placed primary emphasis on the collection of circular polarization data, so there is approximately three times more data for circular polarization than for linear polarization. The radar used a 15-cm-diameter lens antenna, with a one-way beamwidth of 1.5°.

The radar DAS has six I/Q detectors for the monopulse sum and difference signals. The relative phase of the two-sum channels and their log amplitudes are also processed in the DAS. For each transmitted pulse, the signals received in each of the 16 channels are sampled, multiplexed, and digitized by two 12-bit A/D converters. The multiplexed data are transmitted from the radar via a fiber-optic data link to the remote computer-control/recording system at a rate of 240 KB/s. (The latter is a PC that includes an 80486 33-MHz processor, 8 MB of memory, and a 1-GB disc drive.) Data are magnetically recorded on 2-GB 8 mm cassette tapes.

The radar is mounted on a pedestal that can be computer-controlled locally or from a remote station to scan the radar, or to orient it to a fixed position. The pedestal is an elevation-over-azimuth type, with 0.01° pointing accuracy and scanning rates between 0.1 and 10°/s. In addition, a coboresighted video camera mounted on the radar head provides a video record of the scanned area.

## 2.2 Radar Calibration Procedure

The radar calibration procedure is complicated due to the number and types of data channels. The entire procedure has been reported in detail

previously (ref. 2 and 3); therefore, we will discuss only a brief outline of the calibration procedure specific to these measurements. We performed preliminary calibrations in the Laboratory before taking the radar to the field-measurement site at Grayling, and we did a series of premeasurement checks and calibrations at the field test site. The basic features of these checks and calibrations [4] included taking proper account of gain imbalances in I/Q detectors, and nonlinear responses in detectors and amplifiers.

We performed the radar calibrations at the field-measurement site using the reflectors listed in the calibration target array of table 1. We chose the range and the RCS of reflectors 3, 4, and 5 so that the received-signal levels from the reflectors were approximately equal and in the linear range of the receivers (about 6 dB below A/D saturation). We used reflectors 1 and 2 for determining a sign in the PDM calibration described below, for circular and linear polarization, respectively.

We used the PDM calibration technique [5] to compensate for the effects of imperfect cross-polarization isolation in the radar. This calibration method is intended to remove the effects of the radar system parameters from the data so that the target polarization scattering matrix can be determined without degradation due to the system. It can be used for both linear and circular polarization by measuring the five reflectors listed in table 1. For this report, we carried out the PDM calibration technique separately for both circular and linear polarization.

For PDM calibration purposes, depending on the polarization, we selected four of the five reflectors and took 200 ramps of data. (A ramp of data consists of 64 pulses separated in frequency by 10 MHz that are transmitted with 1 polarization, and 64 pulses transmitted with the orthogonal polarization for the 10-MHz step-size data, or 128 pulses transmitted at each polarization for the 5-MHz step-size data.) The first step in processing the PDM data is to perform the I/Q corrections. We generated the I/Q corrections by characterizing each I/Q detector at four different amplitude levels at 22.5° phase intervals, from 0° to 360°. This I/Q correction reduces the residual amplitude error due to I/Q imbalance to 40 dB below the signal level; the maximum required phase correction was 3°. We averaged the 200 ramps of data before calculating the PDM coefficients. To properly average the coherent channels in the PDM data, a constant phase for each frequency is required to calculate the correct average amplitude and phase. We applied a motion-compensating algorithm to the data before averaging to minimize any phase variations due to motion of the calibration

**Table 1. Calibration reflector array.**

| Reflector no. | Reflector type | RCS (dBsm) | Range (m) |
|---|---|---|---|
| 1 | Gridded trihedral | 14 | 160 |
| 2 | Dihedral 22.5° | 18 | 190 |
| 3 | Trihedral | 23 | 218 |
| 4 | Dihedral 0° | 26 | 248 |
| 5 | Dihedral 45° | 26 | 280 |

reflectors during the acquisition of 200 ramps of data. We then calculated the PDM correction parameters for each frequency and for each polarization from the averaged data. We carried out this calibration procedure before and after all data runs, and used the average of these calibrations for calibrating the data for the first Grayling test. The calibration data were acquired as part of the scan data for Yuma and the second Grayling test.

The cross-polarization isolation of the radar was between 25 and 30 dB across the frequency band, and the improvement in the cross-polarization isolation using the PDM calibration technique was between 5 and 10 dB, depending on the frequency. The improvement due to the PDM calibration technique is limited by the clutter return from the antenna sidelobes, as well as the reflected signal from the corner reflector mounting poles. The resulting cross-polarization isolation of the system was improved to about 35 dB, which is more than adequate for measuring MMW backgrounds, since the cross-polarization ratio for natural backgrounds was found to be less than 10 dB.

We obtained antenna radiation patterns at the test site using the various reflectors. The approximate two-way sum channel beamwidth for the 15-cm lens used for the measurements reported here was 1.0°, and the two-way sidelobe levels were less than 40 dB. We determined the radar monopulse boresight angle for each polarization channel, using the appropriate reflector. We found that the boresights for the different polarization combinations varied slightly, with most of the variations in the azimuth. The overall boresight angle difference for the RR and RL channels, for example, was about 0.1°, with most of the difference in the azimuth. We set the optical boresight on the video camera to coincide with the average of the individual boresights.

## 2.3 Clutter Background Measurement Procedure

The high-intensity measurement areas at Grayling and Yuma were outfitted with a full array of meteorological equipment for the SWOE program by other laboratories in order to obtain standard meteorological data, as well as measurements of solar radiance, soil moisture, soil temperature, and cloud conditions. In addition, snow depth and snow density were measured in Grayling, when appropriate. The measurement area in Grayling was 100 by 100 m, and was located at the bottom of a small valley. The radar was positioned on top of a hill overlooking the valley so that the measurement area could be scanned effectively. For Yuma, the radar was mounted on top of a 12-ft-high platform overlooking the two measurement areas, defined as the Thermal Imaging Processing System (TIPS) and Atmospheric Sciences Laboratory (ASL) fields of view. These measurement areas were located on either side of the platform; the calibration reflectors were located midway between the two measurement areas.

At Grayling I and Yuma, we scanned the measurement areas using a raster pattern covering an azimuth increment of 1.2°, an elevation increment of 1.0°, and a range interval of 150 m in 15 m increments. The raster pattern slightly overscanned the areas in azimuth. For the Grayling II test, we increased the azimuth overscan by using 1.0° azimuth steps; we also reduced

the elevation steps slightly. The total azimuth scan varied from 30° to 50°, depending on the test site. We used range overlaps to keep reductions in the measured RCS caused by the sum channel beam shape function to a minimum over the entire area. During the first two tests, we recorded 32 ramps of data for each azimuth, elevation, and range gate. (As discussed previously, each ramp consists of 128 transmitted pulses.) During the second Grayling test, we reduced the frequency step size to 5 MHz, and transmitted 256 pulses during each ramp. This step allowed us to use anti-aliasing techniques to generate high-resolution RCS maps. In addition, we recorded only 8 ramps of data for each cell location. At each angular position, we swept the radar range gate through the range interval, and then incremented the azimuth angle. When all azimuth angles had been measured at one elevation angle, we incremented the elevation position. The depression angles varied from 5° to 1° for both tests. We continued this process until we had measured the entire scan pattern.

We took the MMW measurements at Grayling I over 25 2-hour time periods, randomly selected from 19 to 23 September and 17 to 23 October. During the two hours, we made three complete scans (or data runs) with circular polarization, and one data run with linear polarization. The raw data file included the six coherent I/Q monopulse data channels, the two logarithmic sum channels, and the relative polarimetric phase I/Q channel. The final calibrated data set includes 72 circular and 22 linear polarization runs. The Yuma data set includes 201 circular and 27 linear runs taken over a 47-day period, while the Grayling II data set includes 268 circular and 140 linear runs taken over a 43-day period. Since the same cells were measured again and again for different environmental conditions and times, the data provide a good basis for validation of a SWOE MMW background model.

# 3. Data Discussion

## 3.1 RCS Variations

In order to evaluate the effects of various environmental conditions on the measured RCS for the three different field exercises, we selected a small subset of the measured cells from the radar scan pattern from each test for further analysis, and identified them so that each background type was represented. The background types in the selected cells were grass and bushes, dirt and grass, coniferous trees, and deciduous trees for the Grayling tests; and grass, brittle bush, creosote bush, mixed bushes, and saguaro cactus for the Yuma tests. Since the trees are not, in general, large enough to fill an entire radar cell, the cells identified as a coniferous or deciduous tree may also include some data from grass or dirt, which will have a slight effect on the absolute RCS measurements of the various cell types. We averaged the measured RCS in square meters at each frequency over all ramps of data for each individual cell to compute the cell average for each data run. We then converted the RCS to the RCS per unit area ($\sigma^0$) by dividing by the beam area intersecting the ground at the cell range. We averaged the values and used them to compute the average of $\sigma^0$ in $m^2/m^2$ and the standard deviation in dB space for each cell for the entire measurement period. Tables 2 and 3 give the composite RCS statistics and standard deviation for these selected cells from the Grayling field tests for both circular and linear polarization, respectively.

The individual cell statistics shown in tables 2 and 3 can be used to make some general statements about the cell RCS's for both circular and linear polarization at the Grayling site. It is apparent that the LR and RL RCS values are about equal, and that the RR and LL RCS values are also about equal for all cell types. Also, the LR RCS is about 4 dB larger than the RR

Table 2. Mean RCS dB ($m^2/m^2$) and standard deviations in dB for selected cells for circular polarization from Grayling field tests.

| Cell type | Location | RR | LL | LR | RL |
|---|---|---|---|---|---|
| Dirt and grass | Gray I | −23.1 ± 1.9 | −23.0 ± 1.9 | −19.2 ± 1.5 | −19.1 ± 1.5 |
| Grass and bushes | Gray I | −24.5 ± 2.4 | −24.6 ± 2.5 | −20.6 ± 1.8 | −20.7 ± 1.8 |
| Coniferous | Gray I | −22.2 ± 1.1 | −22.2 ± 1.2 | −18.1 ± 1.4 | −18.3 ± 1.2 |
| Deciduous | Gray I | −23.6 ± 3.5 | −23.3 ± 3.5 | −16.8 ± 3.9 | −17.2 ± 4.0 |
| Grass 1 | Gray II | −24.0 ± 3.8 | −23.5 ± 4.0 | −21.4 ± 2.2 | −21.2 ± 2.2 |
| Grass 2 | Gray II | −24.4 ± 3.3 | −24.3 ± 3.4 | −21.2 ± 1.9 | −21.1 ± 1.8 |
| Grass 3 | Gray II | −25.3 ± 3.6 | −24.6 ± 3.7 | −22.9 ± 2.1 | −22.4 ± 2.1 |
| Grass 4 | Gray II | −22.4 ± 4.3 | −22.4 ± 4.6 | −20.7 ± 2.5 | −20.5 ± 2.5 |
| Grass and coniferous | Gray II | −25.1 ± 2.0 | −22.2 ± 2.2 | −20.6 ± 1.4 | −20.4 ± 1.3 |
| Coniferous 1 | Gray II | −19.0 ± 2.0 | −18.7 ± 2.0 | −15.9 ± 1.3 | −15.6 ± 1.3 |
| Coniferous 2 | Gray II | −22.6 ± 2.0 | −20.7 ± 2.0 | −19.0 ± 1.4 | −18.4 ± 1.3 |
| Coniferous 3 | Gray II | −20.1 ± 2.0 | −20.1 ± 2.0 | −17.1 ± 1.3 | −16.8 ± 1.3 |
| Grass and deciduous | Gray II | −22.2 ± 3.2 | −21.2 ± 3.4 | −19.3 ± 2.1 | −18.9 ± 2.1 |
| Deciduous 1 | Gray II | −20.1 ± 2.7 | −19.7 ± 2.2 | −16.6 ± 1.4 | −16.4 ± 1.3 |
| Deciduous 2 | Gray II | −21.2 ± 2.9 | −21.0 ± 2.6 | −17.6 ± 1.4 | −17.3 ± 1.3 |
| Deciduous 3 | Gray II | −23.0 ± 2.1 | −22.5 ± 2.1 | −19.0 ± 1.4 | −18.8 ± 1.4 |

**Table 3. Mean RCS dB ($m^2/m^2$) and standard deviations in dB for selected cells for linear polarization from Grayling field tests.**

| Cell type | Location | VV | HH | HV | VH |
|---|---|---|---|---|---|
| Dirt and grass | Gray I | −18.3 ± 1.7 | −18.0 ± 1.7 | −25.8 ± 2.3 | −25.8 ± 2.4 |
| Grass and bushes | Gray I | −19.3 ± 1.9 | −19.6 ± 1.9 | −27.3 ± 2.6 | −27.3 ± 2.7 |
| Coniferous | Gray I | −17.6 ± 1.0 | −17.5 ± 1.0 | −24.5 ± 1.2 | −24.5 ± 1.4 |
| Deciduous | Gray I | −16.4 ± 2.3 | −15.8 ± 2.5 | −25.8 ± 2.2 | −25.9 ± 2.4 |
| Grass 1 | Gray II | −20.3 ± 2.5 | −20.2 ± 2.6 | −27.4 ± 3.9 | −27.3 ± 3.9 |
| Grass 2 | Gray II | −20.1 ± 2.1 | −20.5 ± 2.1 | −28.5 ± 3.2 | −28.5 ± 3.3 |
| Grass 3 | Gray II | −21.4 ± 2.6 | −21.6 ± 2.4 | −29.0 ± 3.4 | −28.7 ± 3.5 |
| Grass 4 | Gray II | −19.2 ± 3.1 | −19.7 ± 2.9 | −26.1 ± 4.6 | −26.0 ± 4.6 |
| Grass and coniferous | Gray II | −21.0 ± 1.5 | −18.3 ± 1.3 | −27.4 ± 2.0 | −27.4 ± 2.0 |
| Coniferous 1 | Gray II | −15.2 ± 1.4 | −15.0 ± 1.3 | −22.6 ± 1.9 | −22.5 ± 1.8 |
| Coniferous 2 | Gray II | −18.9 ± 1.5 | −17.0 ± 1.4 | −25.3 ± 1.8 | −24.8 ± 1.8 |
| Coniferous 3 | Gray II | −16.5 ± 1.4 | −16.1 ± 1.4 | −23.7 ± 2.1 | −23.6 ± 2.0 |
| Grass and deciduous | Gray II | −18.5 ± 2.4 | −17.9 ± 2.4 | −25.8 ± 3.3 | −25.4 ± 3.3 |
| Deciduous 1 | Gray II | −16.0 ± 1.7 | −15.5 ± 1.5 | −24.0 ± 2.3 | −23.8 ± 2.3 |
| Deciduous 2 | Gray II | −17.1 ± 1.8 | −16.3 ± 1.5 | −25.1 ± 2.7 | −24.9 ± 2.7 |
| Deciduous 3 | Gray II | −18.5 ± 1.6 | −18.0 ± 1.5 | −26.7 ± 2.0 | −26.5 ± 2.0 |

RCS for all the cells for Grayling I, except for the deciduous tree, where the ratio (LR/RR) is almost 7 dB. For Grayling II, this ratio is between 2 and 4 dB, with the average about 3 dB. For linear polarization, the RCS's for VV and HH are about equal, and the RCS's for HV and VH are almost identical. In addition, the VV RCS averages about 7 dB larger than the HV RCS for all cell types. The standard deviation values in the tables indicate that the RCS for the deciduous tree cells had the largest variation over the measurement period for Grayling I; however, this variation is due almost entirely to a 6-dB decrease in the average RCS of the deciduous tree cell from the beginning of the test to the end. In general, the grass cells actually had the largest variation in RCS due to changing weather conditions for both tests; for Grayling II, the deciduous tree cells were next, with the evergreen tree cells having the smallest dependency on weather.

To identify the causes of the variation in the measured RCS for individual cells, the RCS data were plotted versus time and compared with the weather data observed at those times. The behavior of the four selected cell types from Grayling I are shown in figure 2, in which the average RCS's for each data run for each cell type are plotted versus run number. The run numbers are sequential in time from the beginning to the end of the measurements. The weather conditions present during the data runs are shown in figure 3. Upon comparison of figure 2 with figure 3, it is apparent that the major variations of the grass cells are primarily due to the presence of water, frost, or snow on the ground. In fact, the largest variation in the RCS for these cells is due to the refrozen-snow condition observed for run number 53. This is shown clearly in figure 4, where the grass cell RCS is plotted on an expanded scale, showing the weather conditions responsible for the significant variations. The RCS's for the coniferous trees were somewhat less sensitive to these conditions, but the effects were still evident. The RCS for the deciduous tree seemed to be less sensitive to the weather, but the RCS decreased as the leaves changed color and lost moisture. The results for linear polarization are similar, and will not be discussed here.

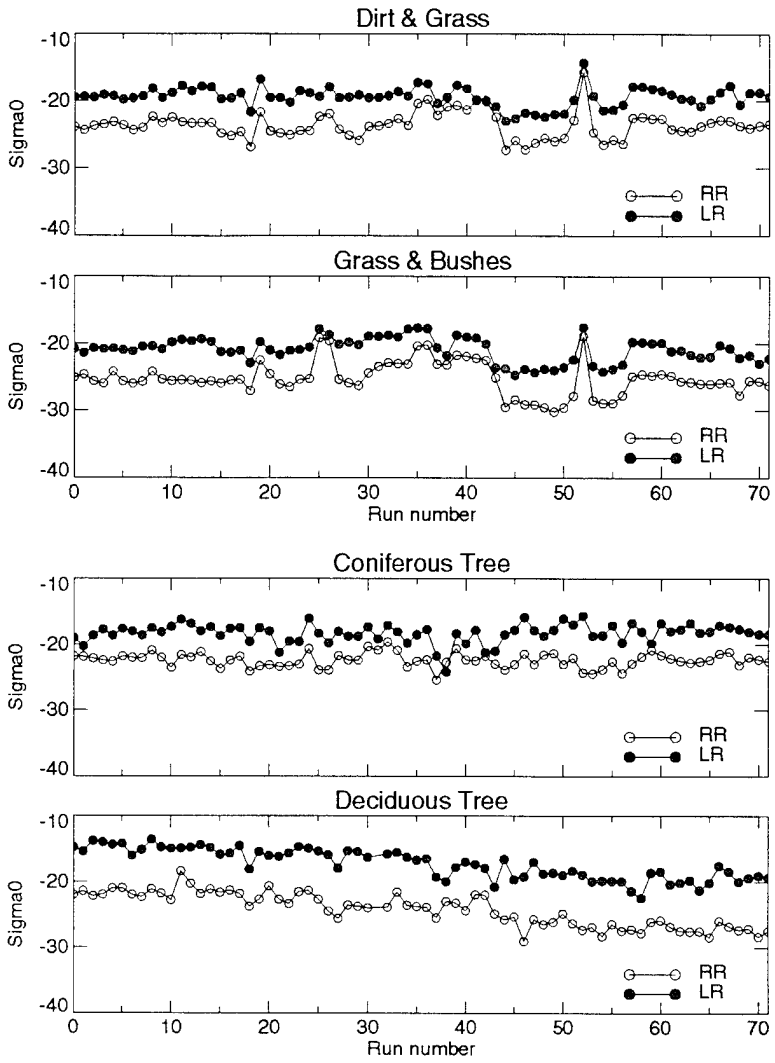


**Figure 2. Graphs of sample cell RCS ($\sigma^0$) versus run number for Grayling I test.**

The Grayling II field-test data were taken during the time period from early March to mid April. During this time, there was a considerable amount of snow cover—both fresh snow and refrozen snow were present during the missions. The presence of the snow had a considerable impact on the measured RCS of the grass cells, with slightly less of an effect on the deciduous tree cells, and little effect on the coniferous tree cells. To understand and compare the measurement results between cells of the same type and between cells of different types, the RCS data was plotted versus mission number for all the selected cells from Grayling II for both circular and linear polarization. During missions in which more than one data run for linear or circular polarization was measured, the data runs were averaged together to get one data point for each polarization for each mission. The RCS data-versus-mission number for selected cells are shown in figures 5 through 10, with the corresponding weather conditions shown in figure 11. By comparing the weather data with the various RCS plots for specific cell types, the following conclusions can be drawn.

Figure 3. Measured snow depth, precipitation rate, and temperature coincident with Grayling I data runs.

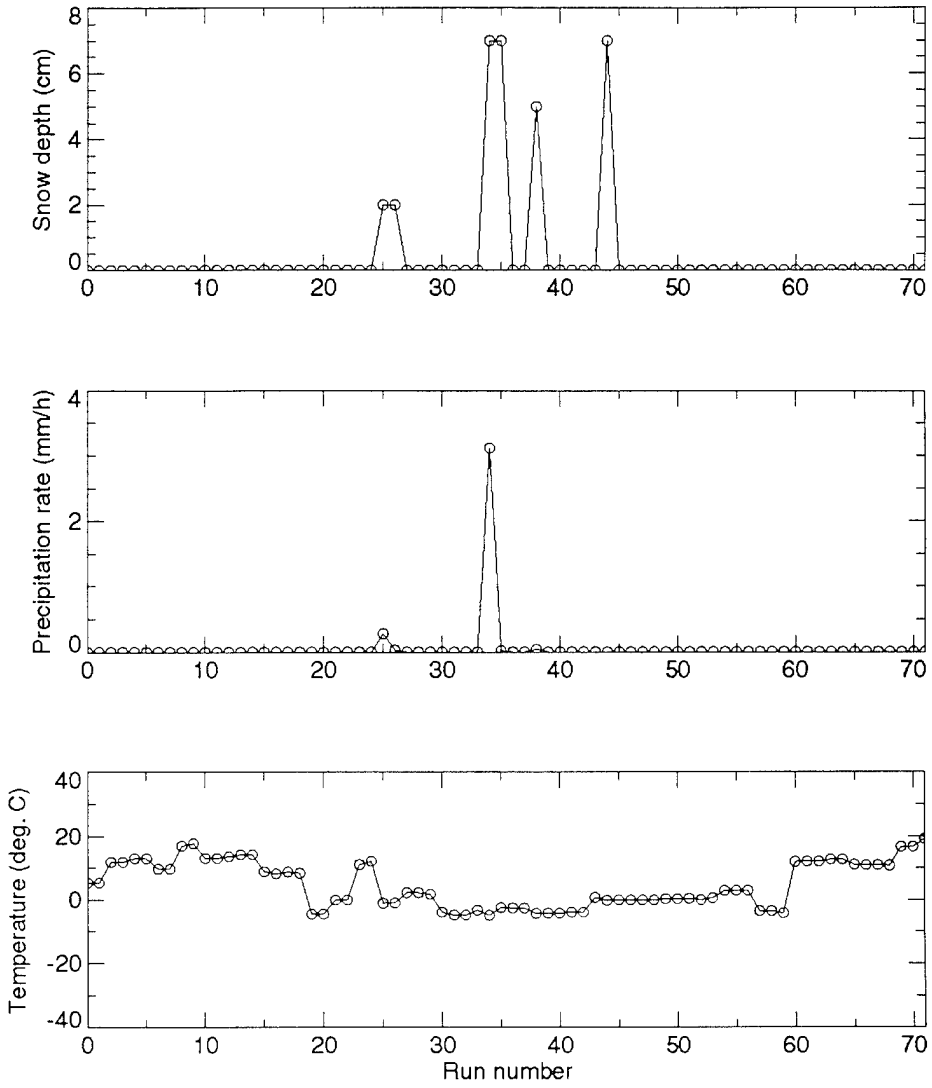


Figure 4. The grass-cell RCS ($\sigma^0$) plotted versus run number with the weather conditions responsible for the variations indicated.

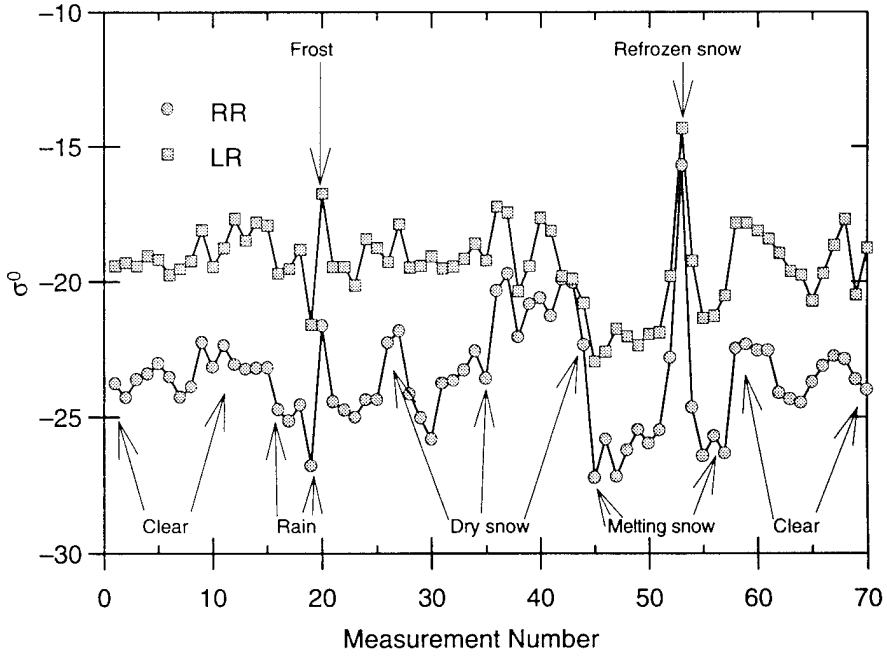

Figure 5. RCS ($\sigma^0$) for indicated cells versus mission number for circular polarization (top) and linear polarization (bottom) for Grayling II test on grass 1 and 2.

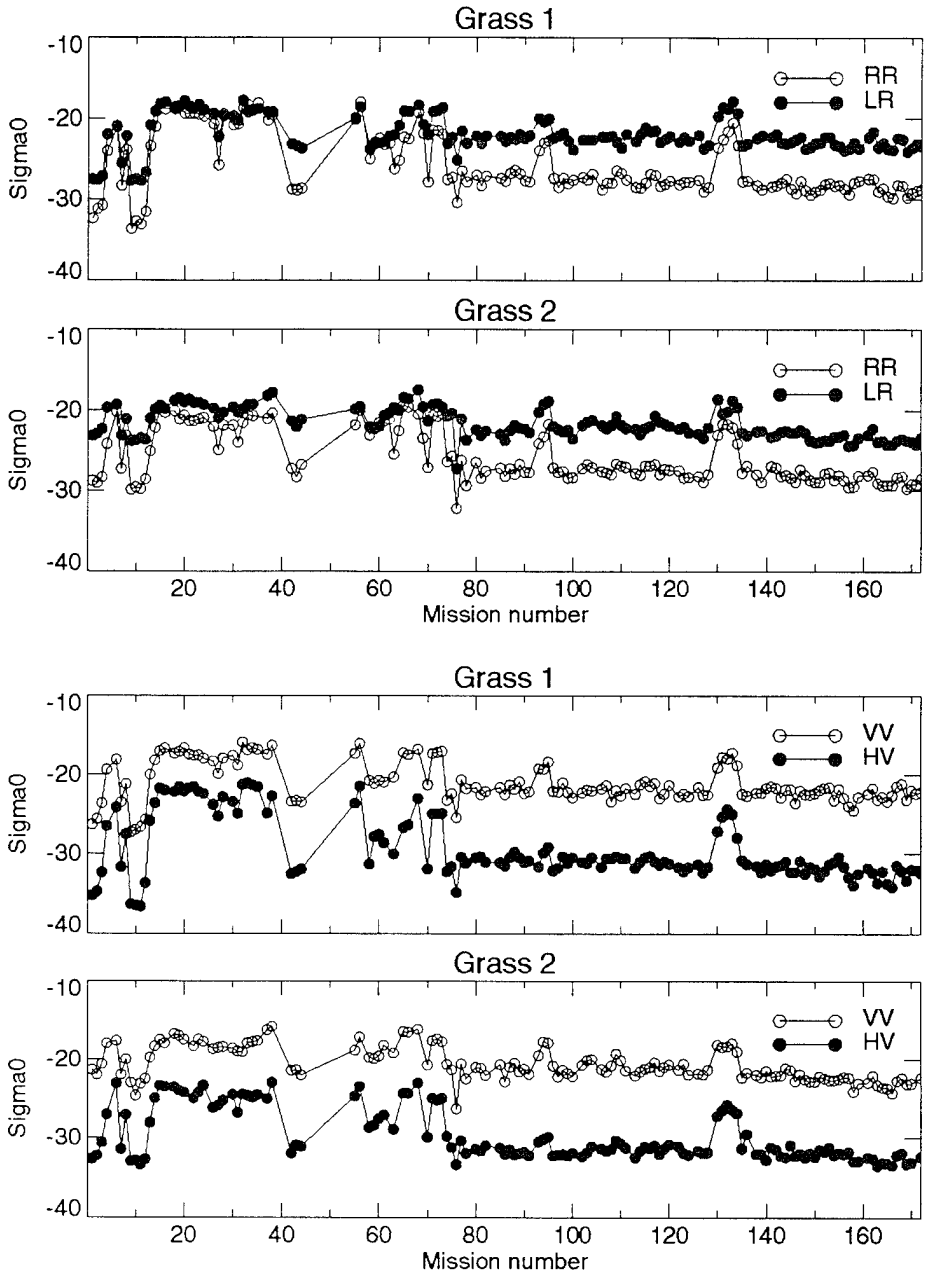

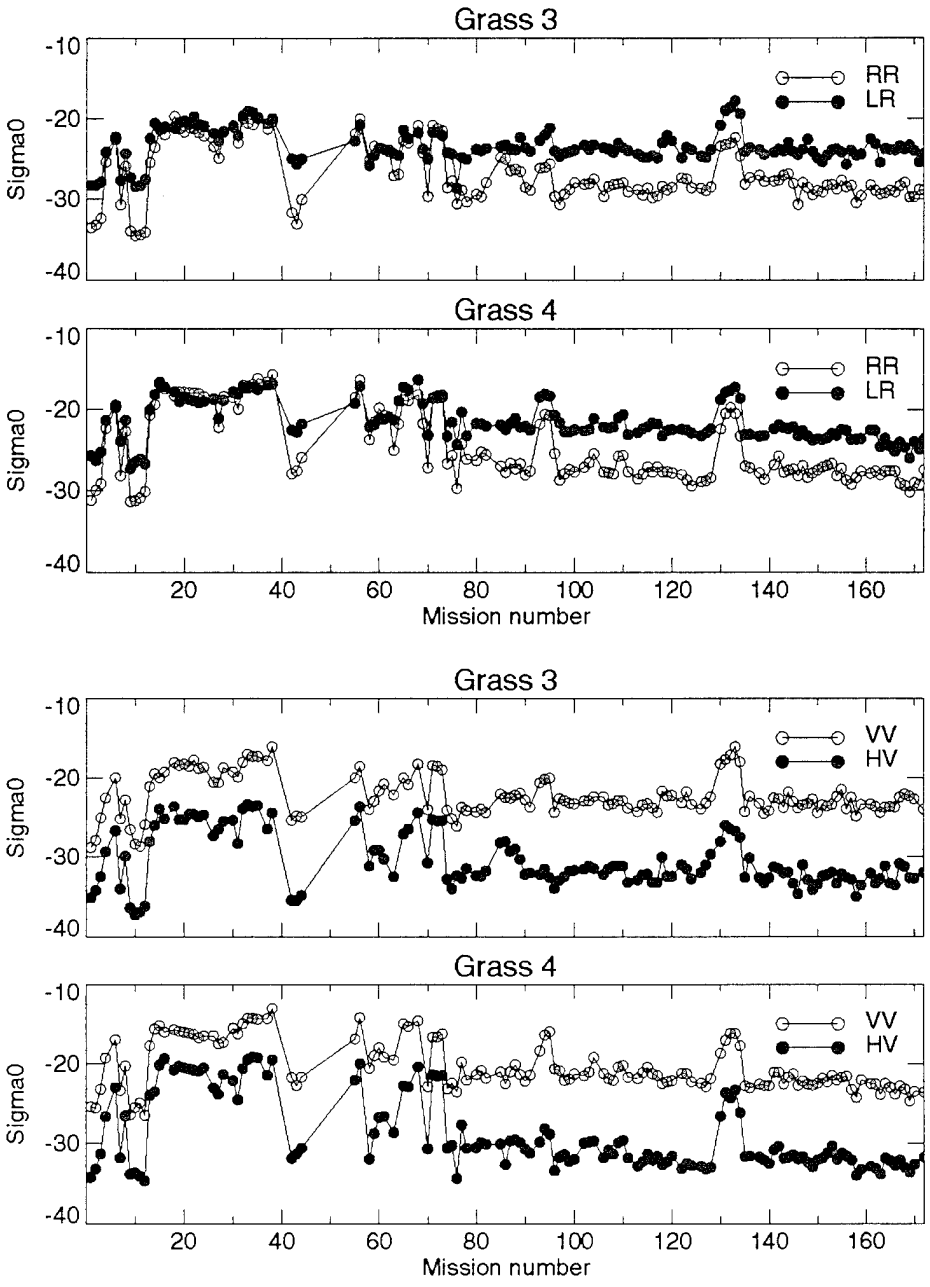


**Figure 6. RCS ($\sigma^0$) for indicated cells versus mission number for circular polarization (top) and linear polarization (bottom) for Grayling II test on grass 3 and 4.**

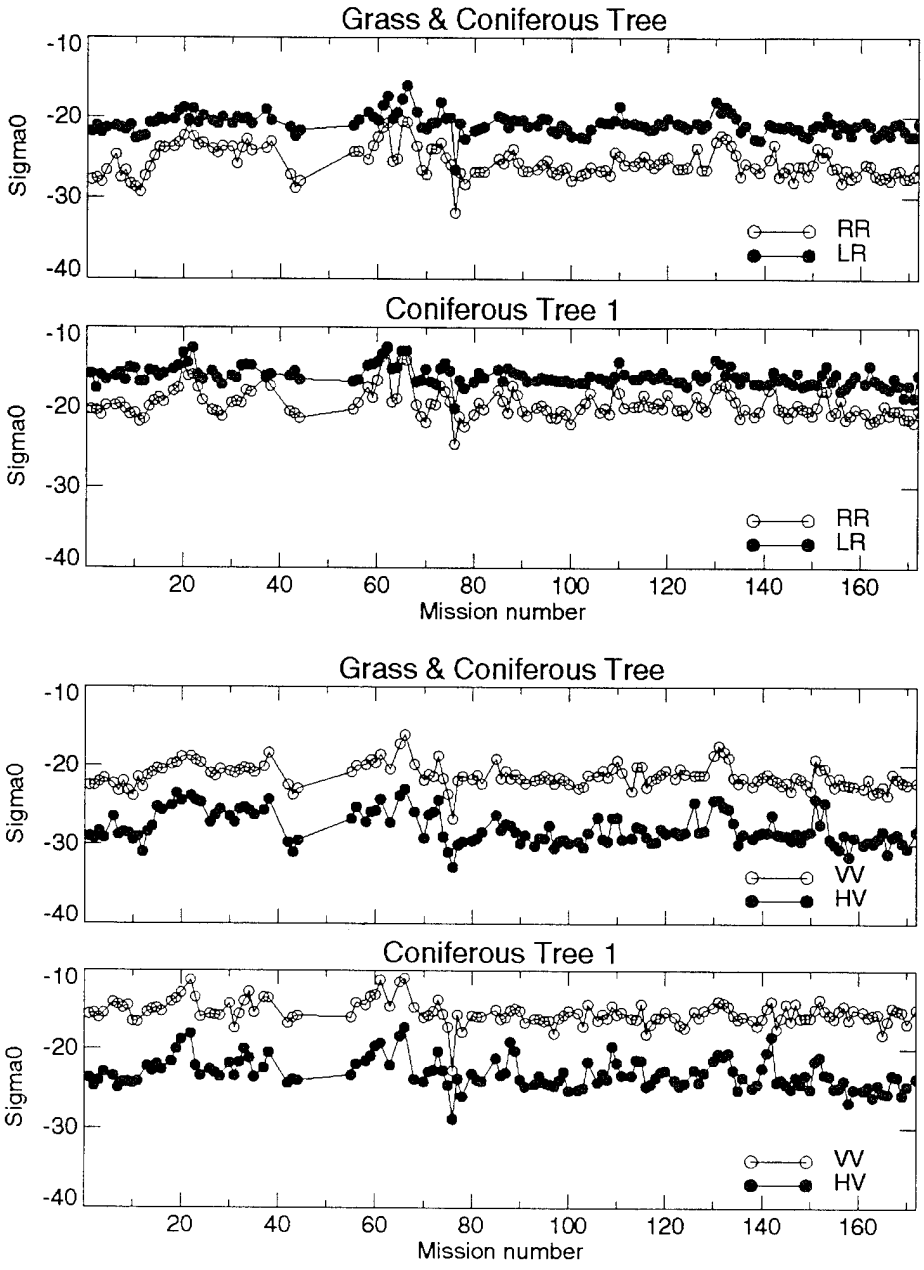


**Figure 7. RCS ($\sigma^0$) for indicated cells versus mission number for circular polarization (top) and linear polarization (bottom) for Grayling II test on grass and coniferous tree.**

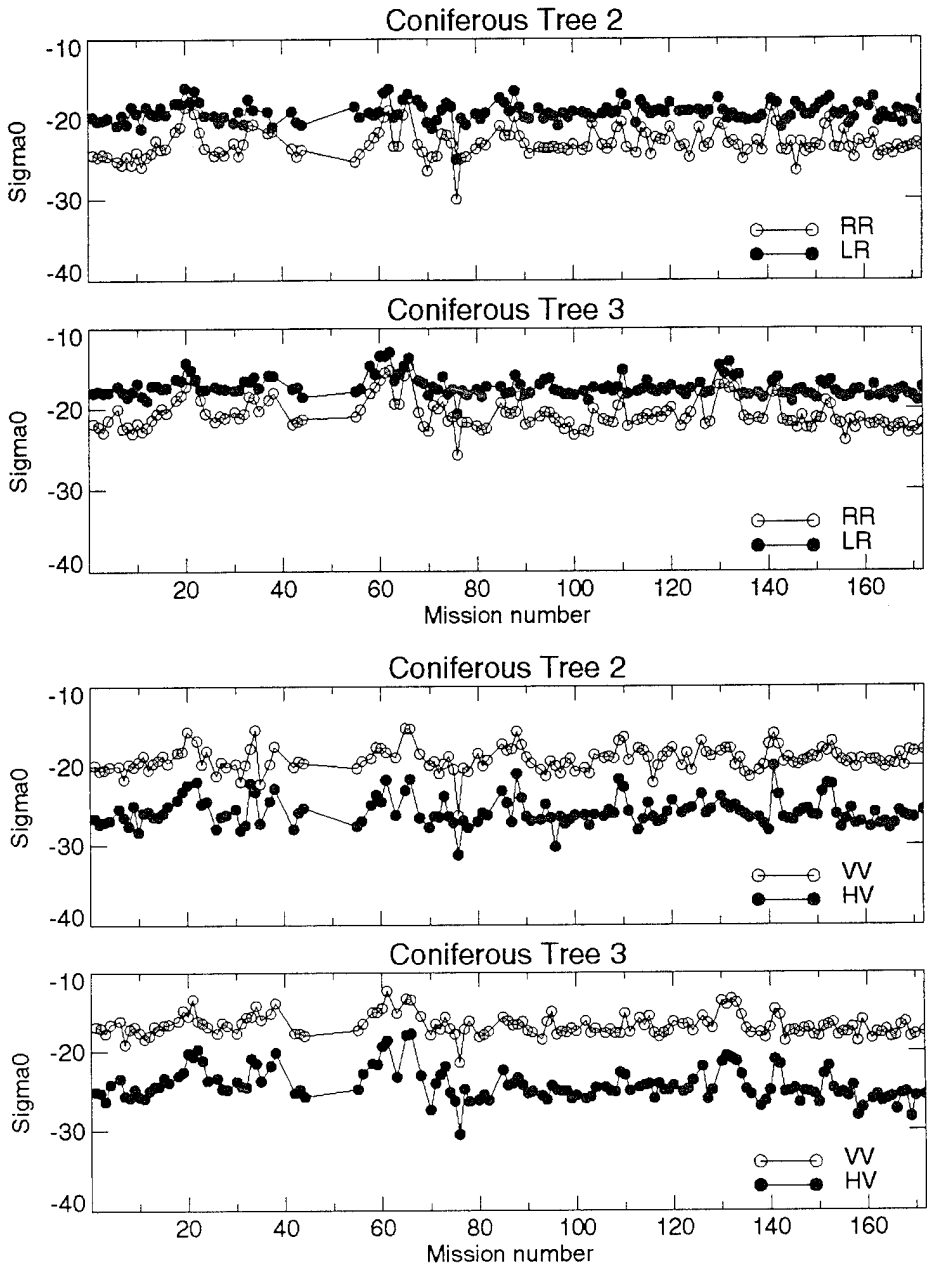


**Figure 8. RCS ($\sigma^0$) for indicated cells versus mission number for circular polarization (top) and linear polarization (bottom) for Grayling II test on coniferous tree 2 and 3.**

Figure 9. RCS ($\sigma^0$) for indicated cells versus mission number for circular polarization (top) and linear polarization (bottom) for Grayling II test on grass and deciduous tree.

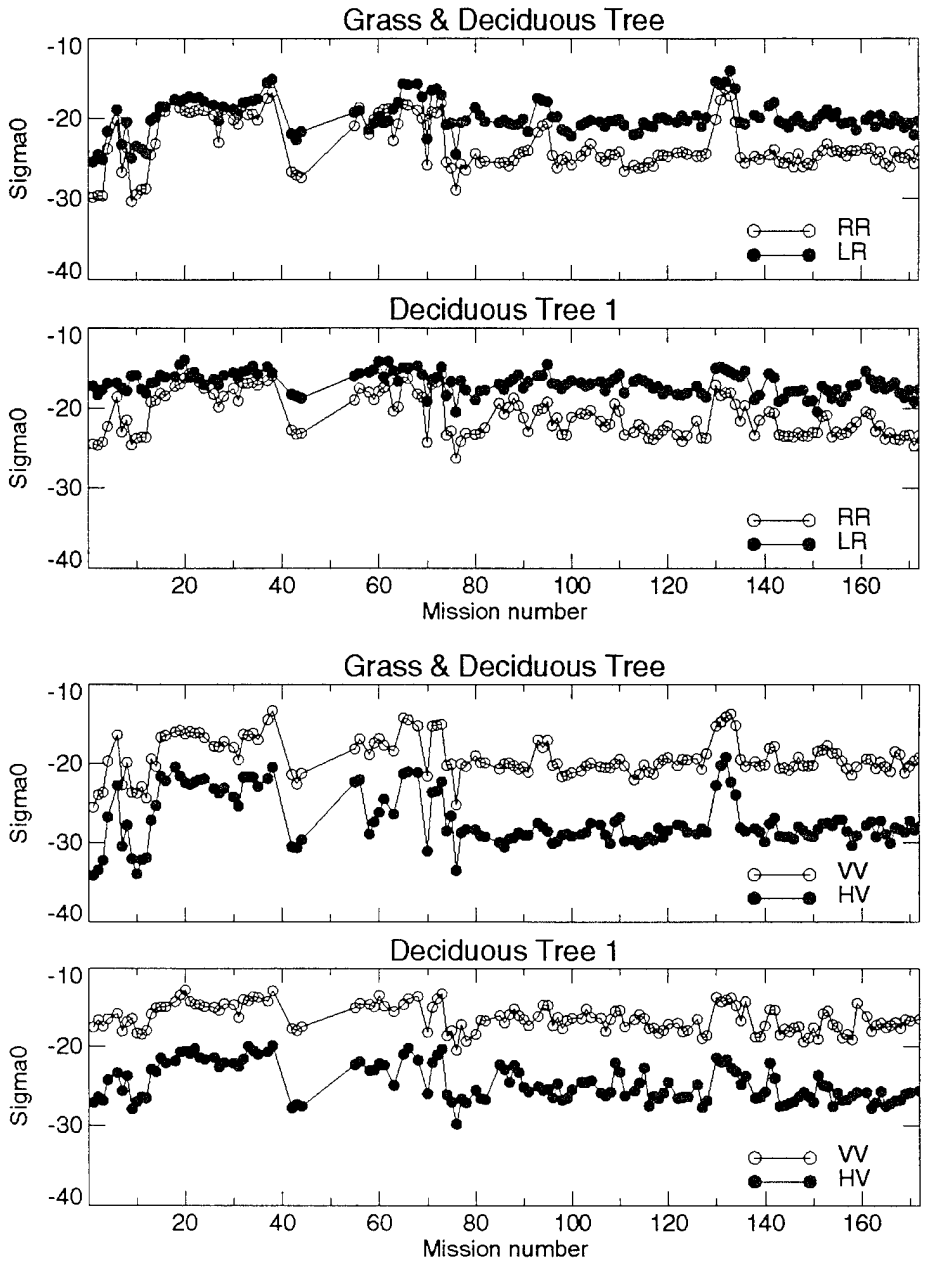

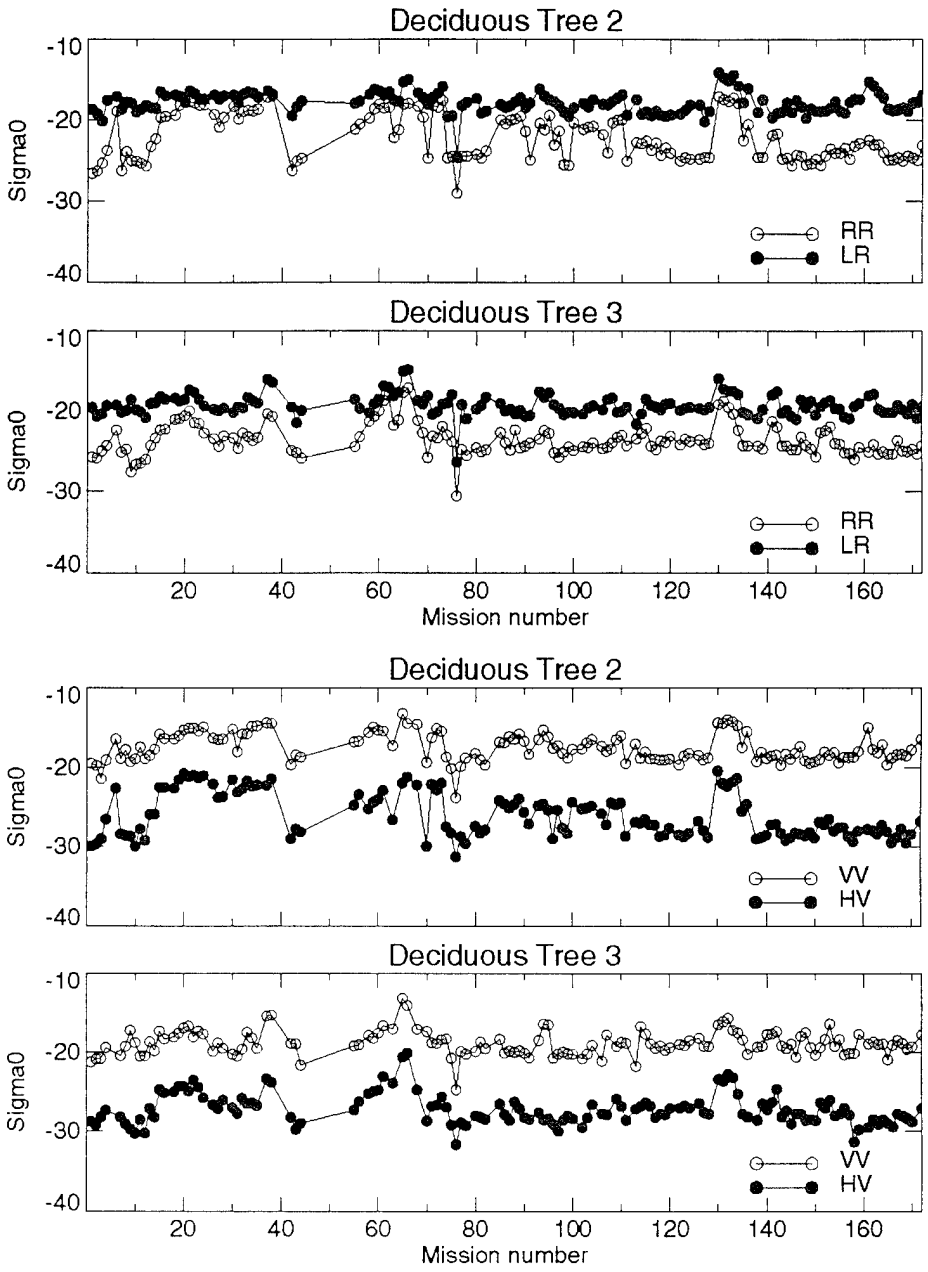


Figure 10. RCS ($\sigma^0$) for indicated cells versus mission number for circular polarization (top) and linear polarization (bottom) for Grayling II test on deciduous tree 2 and 3.

**Figure 11. Measured snow depth, precipitation rate, and temperature coincident with Grayling II missions.**

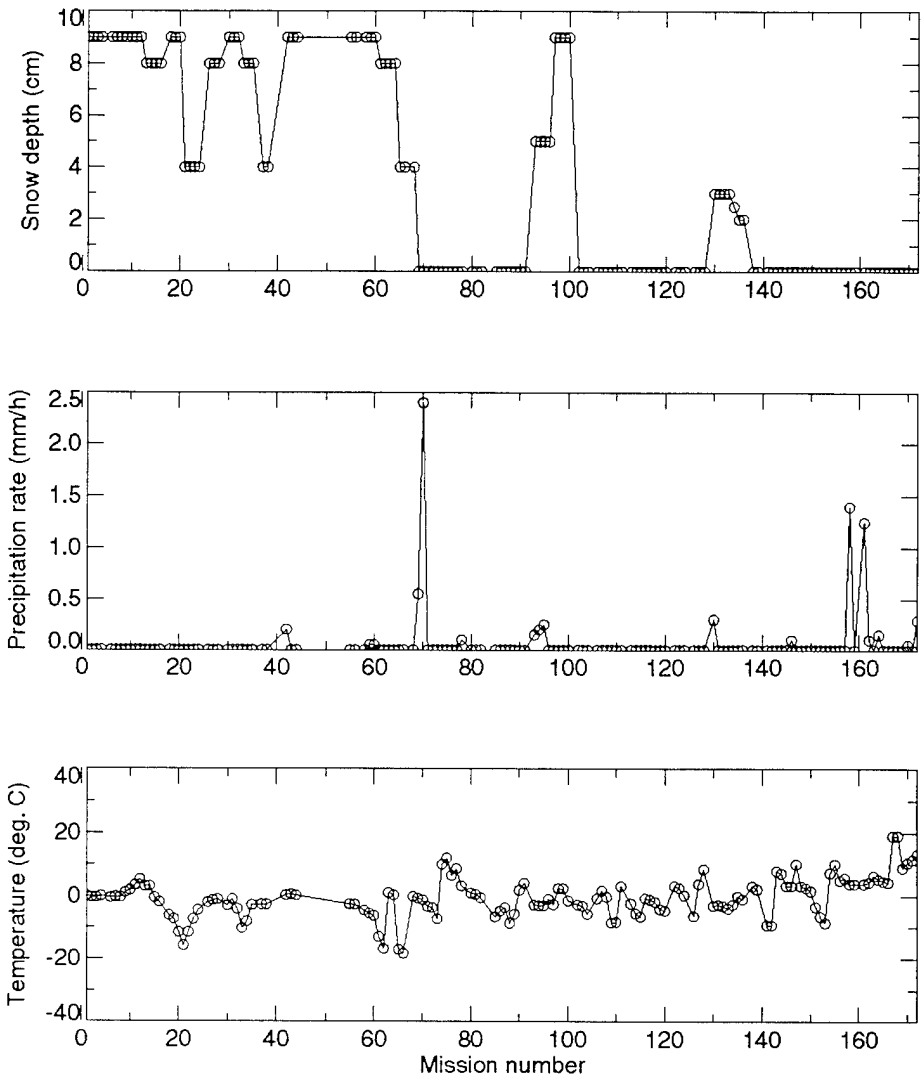

Grass cell RCS is dependent on the amount of snow cover and snow condition present. The RCS of the grass cells was highest for refrozen snow. (Refrozen snow can be assumed to exist whenever there is snow cover and the temperature has risen above freezing and then dropped below freezing.) This occurred from missions 15 to 40 and at a few other missions during the test. For fresh snow, the measured RCS was slightly lower (missions 92 to 94, and 131 to 134). The RCS was the lowest for melting snow when large areas of water accumulated on the ground (missions 9 to 13), and somewhere in between the fresh- and melting-snow conditions for the clear or no-snow-cover condition. The polarization ratio LR/RR was about 3 dB for fresh snow, about 0 dB for refrozen snow, and about 5 dB for no snow. For linear polarization, the polarization ratio VV/HV was about 6 dB for fresh snow, about 4 dB for refrozen snow, and about 8 dB for the no-snow condition. It was also apparent that, for the condition without snow cover, there is a slight decrease in the grass RCS over time, due to the increase in the soil's moisture content that occurs as the ground thaws in the spring. There was no apparent growth in the grass during the test, so that any effect due to the grass growing was minimal. The graphs of the linear and circular polarization exhibit similar behavior over time, and the amplitudes of the individual grass cells track very well over time, with only slight differences in the absolute magnitude of the RCS.

Upon examination of the graphs of the RCS versus mission number for the coniferous tree cells, some interesting features were evident. First of all, the RCS amplitude of the individual cells tracked each other very well over time for both linear and circular polarization. There does not appear to be any overall trend in these measurements, but some slight effects due to fresh snow are apparent (missions 131 to 134), and there are a large number of changes in the RCS that cannot be explained by precipitation and snow cover. The circular polarization ratio generally runs about 3 to 4 dB for the entire test, with a few missions where it drops to around 0 dB. The linear polarization ratio is generally about 7 dB, but drops to around 3 dB when the circular polarization ratio drops. By correlating the coniferous tree RCS measurements to the temperature, we found that there was a measurable increase in the cell RCS for both linear and circular polarization when the temperature dropped below freezing. This effect was probably due to the freezing of the needles and the resulting change in the index of refraction caused by the conversion of the liquid water in the needles to ice. A more in-depth study of this behavior will be conducted in the near future, but is not included in this report.

The graphs of the RCS-versus-mission number for the deciduous tree cells exhibit behavior similar to the grass cells. Since these trees were not fully foliated during the measurement period, the measured RCS is a combination of the ground around the trees and the trees themselves. The magnitude of this effect can be seen by comparing figures 5 and 6 to figures 9 and 10. These figures track each other quite well, especially during the refrozen-snow condition, but the total RCS for the deciduous trees is between 2 and 3 dB higher. This would indicate that the ground is contributing almost half of the total RCS. There is even a slight decrease in the RCS values over time for circular polarization, as was evident in the grass cells.

The polarization ratios for both linear and circular polarization are comparable to those of the grass cells. Although it was not observed, the RCS of deciduous trees should increase as the leaves grow in a similar manner to the decrease shown for Grayling I, when the leaves of the deciduous tree turned brown. To separate the effects of the ground return on the total RCS, analysis is required at a higher range resolution, so that the contribution from the ground can be removed and the contribution from the tree can be isolated. This analysis is planned for the near future.

We started the Yuma field test about mid-March and concluded it at the end of April 1993. Due to the excessive amount of rain that fell during the winter, blooming of the desert occurred well before the first measurement mission. In addition, there was only one rain event during the entire test period. In tables 4 and 5, the composite RCS statistics for selected cells over the entire test period are shown. The data indicate that there was very little variation in the cell RCS's over the test period for all cells except the saguaro cactus. As with the Grayling data, the RL and LR amplitudes are almost identical, and the RR and LL amplitudes are very similar. Likewise, the VH and HV returns are identical for linear polarization, and the VV and HH returns are very similar. The measured cell polarization ratios are also similar to those measured in Grayling I, and slightly higher than those observed in Grayling II for all cells except the saguaro cactus, where the polarization ratios were 6.5 and 16 dB for circular and linear polarization, respectively. The Grayling II polarization ratios were slightly lower for most cells due to the effects of the snow cover and variable weather conditions, which tend to increase the returns for RR and LL compared to RL and LR. To examine the behavior of the cell RCS amplitudes over time for the Yuma test, the RCS's of the selected cells were plotted versus mission number. These plots are shown in figures 12, 13, 14, and 15 for both circular and linear polarization, respectively; corresponding weather data is shown in figure 16.

**Table 4. Mean RCS dB ($m^2/m^2$) and standard deviations in dB for selected cells for circular polarization from Yuma field test.**

| Cell type | Location | RR | LL | LR | RL |
|---|---|---|---|---|---|
| Brittle bush 1 | Yuma | −23.7 ± 0.5 | −23.8 ± 0.6 | −18.9 ± 0.6 | −18.9 ± 0.6 |
| Brittle bush 2 | Yuma | −27.6 ± 0.6 | −27.1 ± 0.7 | −23.1 ± 0.6 | −23.4 ± 0.6 |
| Creosote bush 1 | Yuma | −25.6 ± 0.7 | −26.1 ± 0.7 | −21.8 ± 0.9 | −21.9 ± 0.9 |
| Creosote bush 2 | Yuma | −24.1 ± 0.7 | −24.1 ± 0.8 | −19.3 ± 1.1 | −19.3 ± 1.1 |
| Mixed bushes 1 | Yuma | −24.7 ± 0.8 | −26.2 ± 0.8 | −19.3 ± 1.0 | −19.4 ± 1.0 |
| Mixed bushes 2 | Yuma | −20.1 ± 0.8 | −20.0 ± 0.7 | −15.9 ± 0.8 | −15.9 ± 0.8 |
| Grassy area | Yuma | −29.3 ± 1.9 | −28.5 ± 1.4 | −24.9 ± 1.1 | −24.6 ± 1.0 |
| Saguaro cactus | Yuma | −18.1 ± 2.1 | −18.0 ± 2.1 | −11.6 ± 2.1 | −11.6 ± 2.1 |

**Table 5. Mean RCS dB ($m^2/m^2$) and standard deviations in dB for selected cells for linear polarization from Yuma field test.**

| Cell type | Location | VV | HH | HV | VH |
|---|---|---|---|---|---|
| Brittle bush 1 | Yuma | −17.9 ± 0.4 | −18.1 ± 0.6 | −26.9 ± 0.6 | −26.7 ± 0.5 |
| Brittle bush 2 | Yuma | −22.2 ± 0.6 | −22.0 ± 0.5 | −30.2 ± 0.5 | −30.3 ± 0.6 |
| Creosote bush 1 | Yuma | −20.5 ± 0.8 | −21.3 ± 0.9 | −28.6 ± 0.8 | −28.5 ± 0.8 |
| Creosote bush 2 | Yuma | −17.9 ± 1.1 | −18.2 ± 1.0 | −27.6 ± 0.8 | −27.5 ± 0.8 |
| Mixed bushes 1 | Yuma | −17.8 ± 0.9 | −19.8 ± 0.8 | −28.2 ± 0.6 | −28.1 ± 0.6 |
| Mixed bushes 2 | Yuma | −14.9 ± 0.6 | −14.9 ± 0.7 | −23.1 ± 0.8 | −23.1 ± 0.8 |
| Grassy area | Yuma | −24.1 ± 1.3 | −23.7 ± 1.0 | −32.6 ± 1.6 | −32.1 ± 1.4 |
| Saguaro cactus | Yuma | −8.7 ± 2.2 | −11.4 ± 2.1 | −27.8 ± 2.2 | −27.7 ± 2.1 |

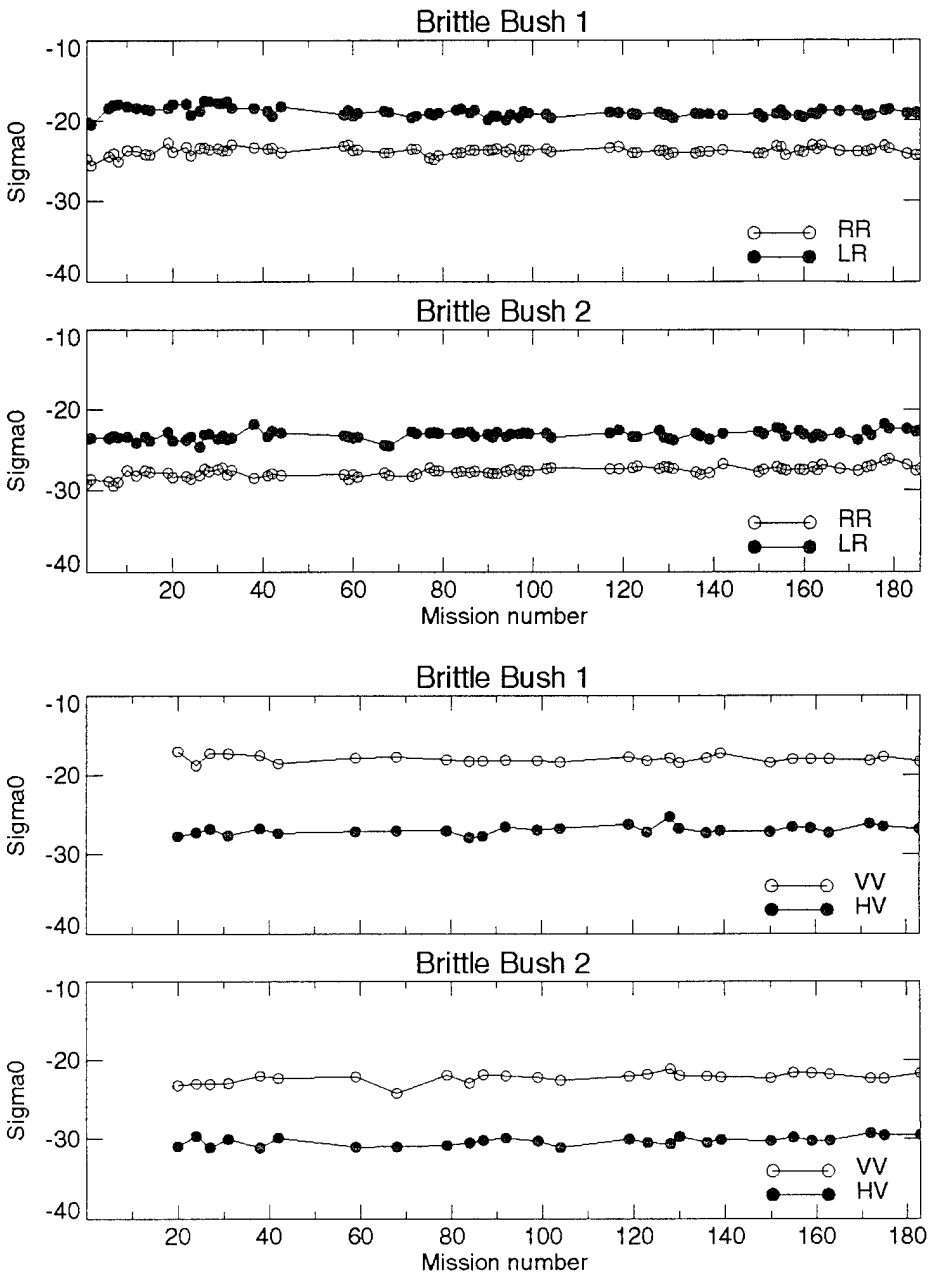


**Figure 12. RCS ($\sigma^0$) for indicated cells versus mission number for circular polarization (top) and linear polarization (bottom) for Yuma test on brittle bush 1 and 2.**

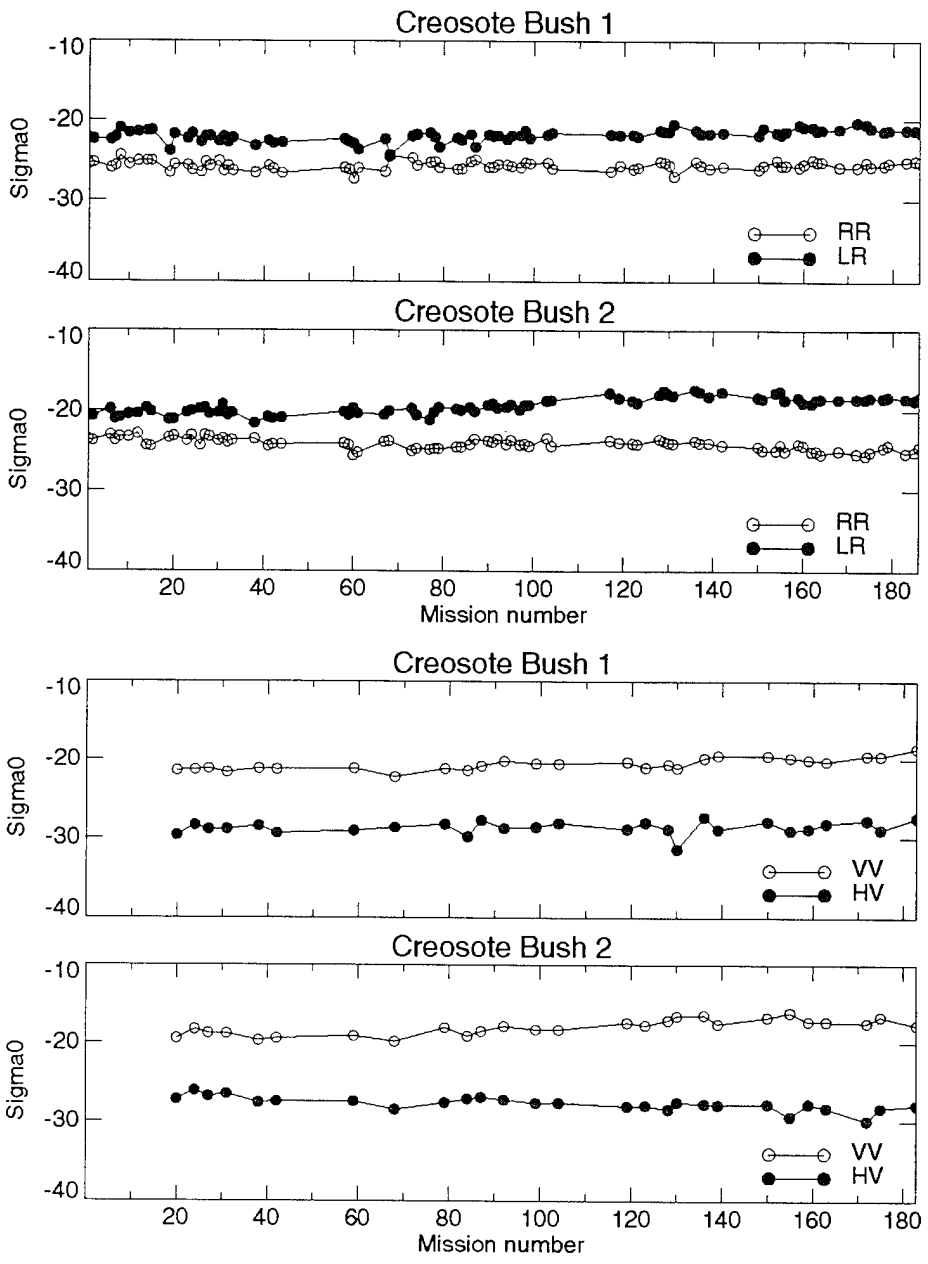


**Figure 13. RCS ($\sigma^0$) for indicated cells versus mission number for circular polarization (top) and linear polarization (bottom) for Yuma test on creosote bush 1 and 2.**

Figure 14. RCS ($\sigma^0$) for indicated cells versus mission number for circular polarization (top) and linear polarization (bottom) for Yuma test on mixed bushes 1 and 2.

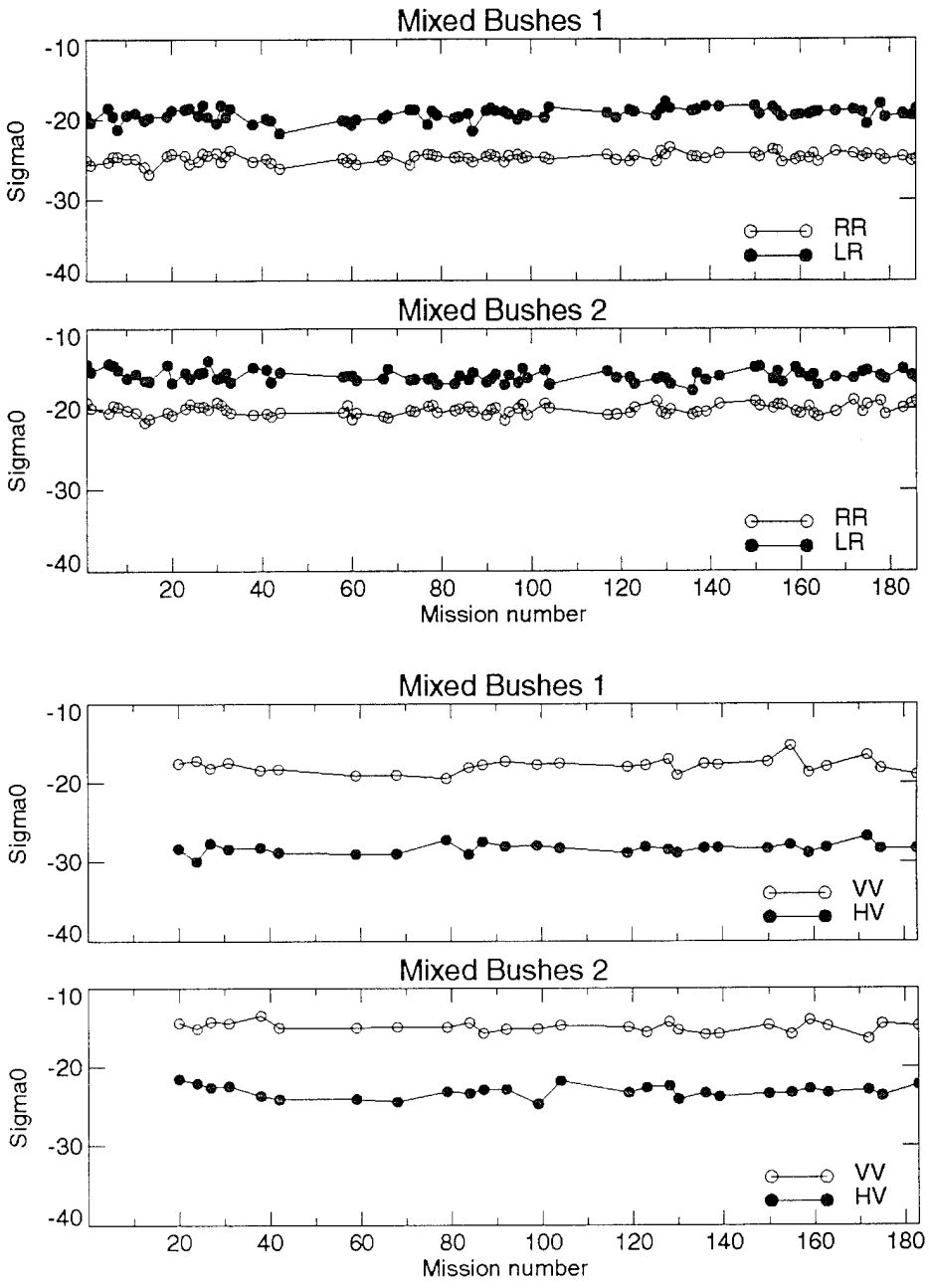

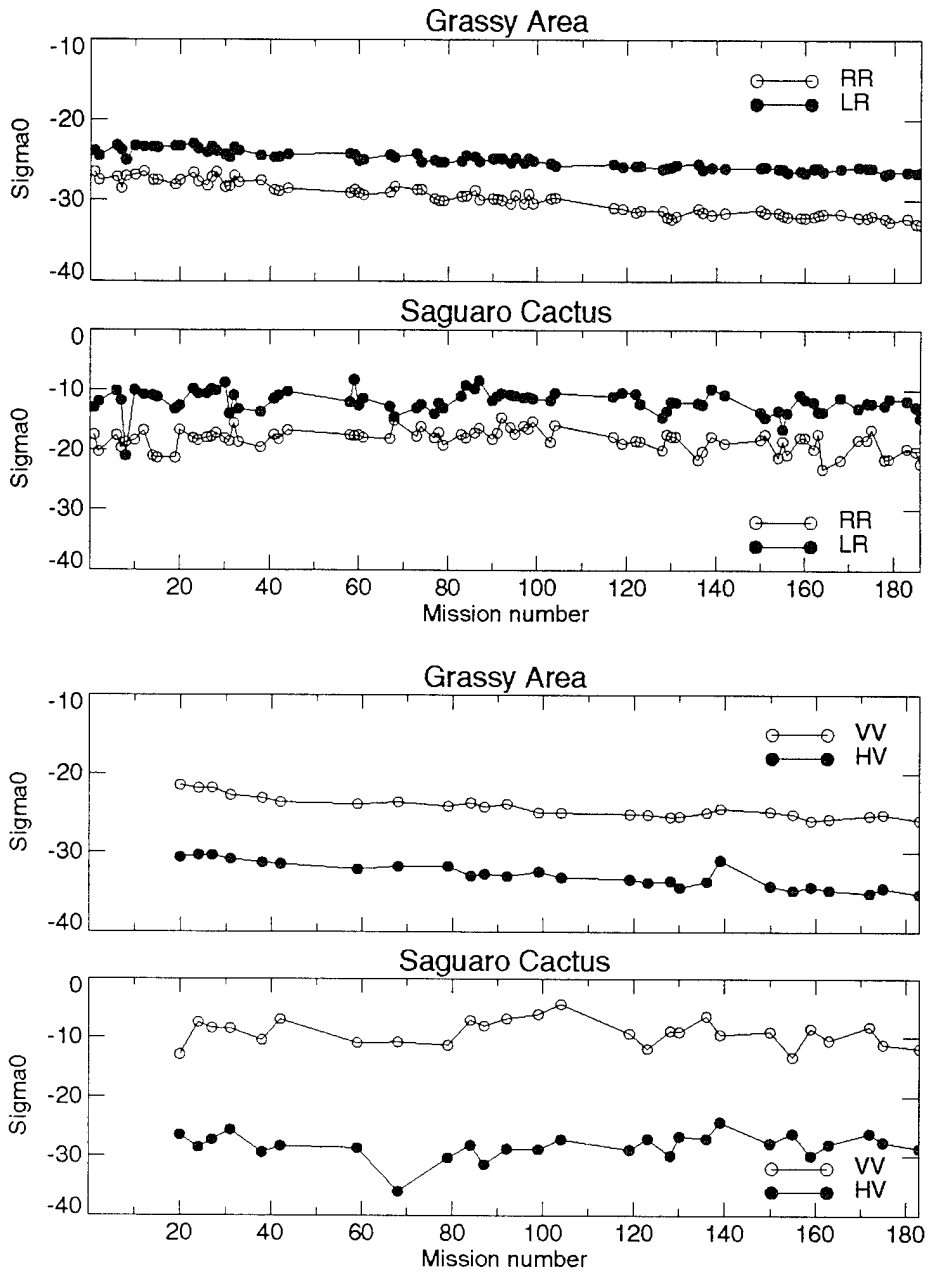


Figure 15. RCS ($\sigma^0$) for indicated cells versus mission number for circular polarization (top) and linear polarization (bottom) for Yuma test and grassy area and saguaro cactus.

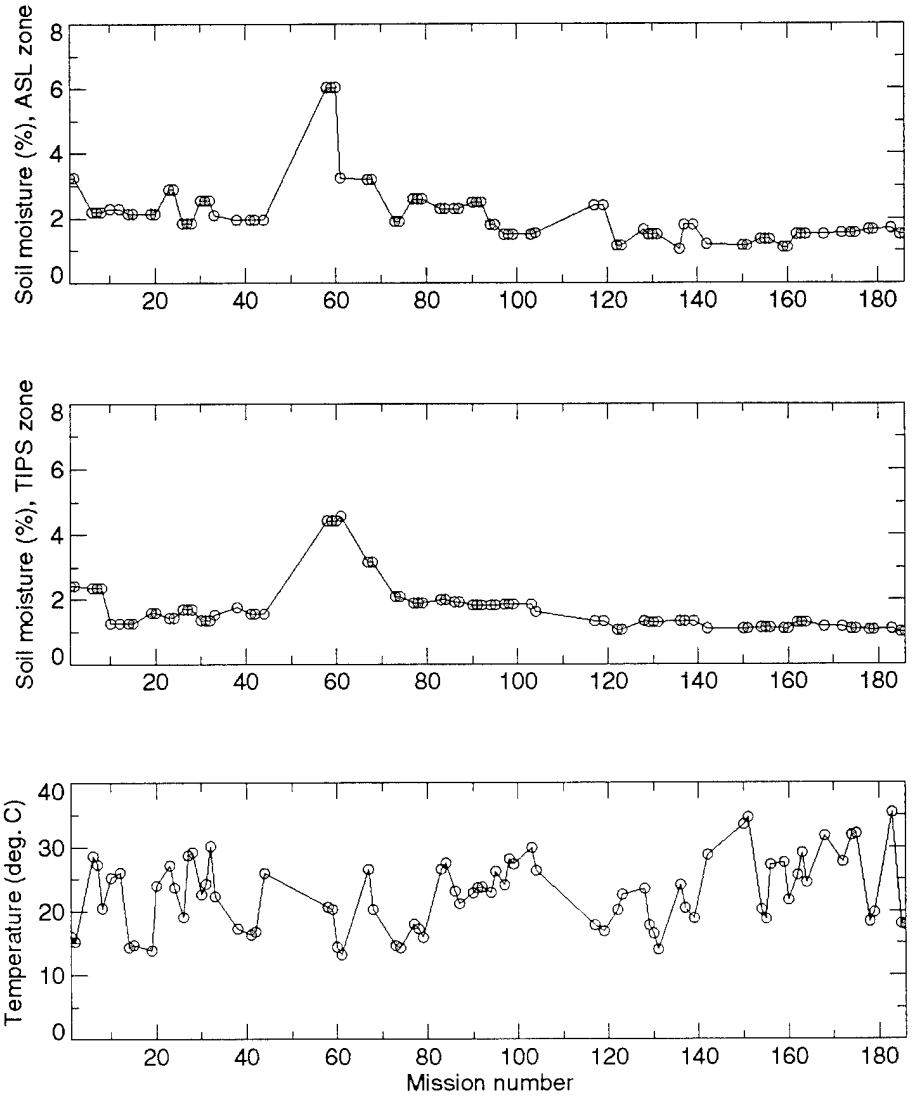


**Figure 16. Measured soil-moisture levels averaged over the ASL and TIPS sites and temperature observed during missions at Yuma.**

The graphs of the cell RCS's for the bushes shown in figures 12 to 14 show very little variation in the cell amplitudes over the measurement missions. The grassy area in figure 15 shows a slight decrease in the RCS over time, due in part to a decrease in the moisture content of the grass as it turned brown during the test. The saguaro cactus (also shown in fig. 15) exhibited large excursions in the measured RCS for both linear and circular polarization over the various missions. This effect was even larger than indicated by the figure when the individual data runs were compared instead of the mission averages. At first, this effect was puzzling, but after carefully examining the data, we determined the cause of these variations: the variations were caused by the motion of the cactus in the wind. When there was little or no wind, the measured RCS was relatively stable. However, when the wind blew strongly, there were wild variations in the measured RCS. The cactus is, essentially, a combination of cylinders oriented vertically, and the radar illuminates the cactus almost perpendicular to the long dimension of these cylinders. These multiple cylinders produce an interference pattern over the bandwidth of the radar and this pattern varies, depending on the absolute orientation of the cylinders. This effect is the

cause of the very high linear polarization ratio. In addition, the cactus presents a large aperture to the radar and, consequently, because of diffraction, generates a very narrow reflection pattern. A slight variation in the angle of illumination of the cactus can cause a large variation in the interference and the reflection pattern characteristics. These effects occur when the wind causes the cactus to bend or to slightly change position in the wind. The weather data indicates a slight increase in the soil moisture at mission 60. This change took place as a result of the only rainfall during the entire test. The soil-moisture levels were very low over the entire test period, with an overall decrease over time. By examining the data carefully, we found no obvious trends that could be attributed to soil moisture, humidity, or temperature. To isolate the different environmental effects, we performed the more in-depth analysis described below.

## 3.2 Clutter Distribution Analysis

We also used the collected data to generate RCS histograms of sample clutter cells for RR and RL polarization. We compiled these histograms from over 1800 individual RCS measurements made across the radar bandwidth for each cell from the Grayling I and Yuma tests, choosing the files to give a representative comparison of distributions for the different clutter types. The histograms are shown in figures 17 and 18, where the number of measurements occurring in a 1-dB bin is plotted versus the measured RCS per unit area ($\sigma^0$) of the bin. It was apparent that each type of clutter cell had about the same distribution function for both polarizations, with a slight difference in the mean value of the distribution. The distribution function for this type of histogram is dependent on the number and magnitude of the individual scatterers in the clutter cell. For instance, the distribution for a single large scatterer (e.g., a corner reflector) would be narrowly peaked about the reflector RCS value. Distributed clutter would have a wider distribution similar to those shown in the figures. Since the grass cells seem to exhibit the most variation due to changing weather conditions, we generated comparison histograms for the dirt and grass cells for different weather conditions. These histograms are shown in figure 19 for both RR and RL polarizations. The figures show the distributions at the beginning and end of the measurements, for frost and refrozen snow. The histograms for this particular cell were essentially the same for the beginning and the end of the test, while the frost condition modified the distribution only slightly. However, the refrozen-snow condition distributions for both polarizations became more irregular with large peaks, compared to the beginning distributions.

The distribution for both polarizations was almost the same for this case, as well. Analyses of the histograms for the other cell types indicated that the distributions did not change significantly during the test. These results suggest that a single type of distribution function should be able to describe the clutter for all conditions, with the exception of refrozen snow. Further analysis is needed to determine the appropriate functions for describing the statistics of individual clutter cells, and for determining a distribution function that best describes the entire clutter area.

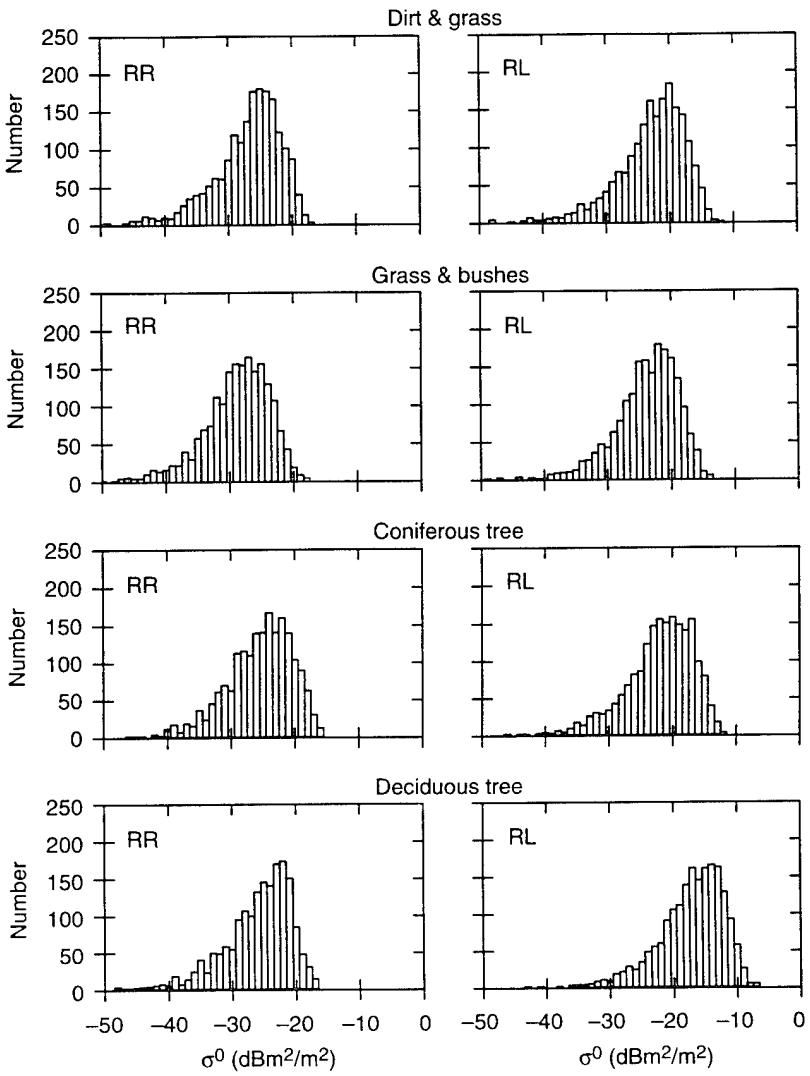


**Figure 17. Sample histograms for Grayling I clutter types for RR and RL polarization.**

**Figure 18. Sample histograms for Yuma clutter types for RR and RL polarization.**

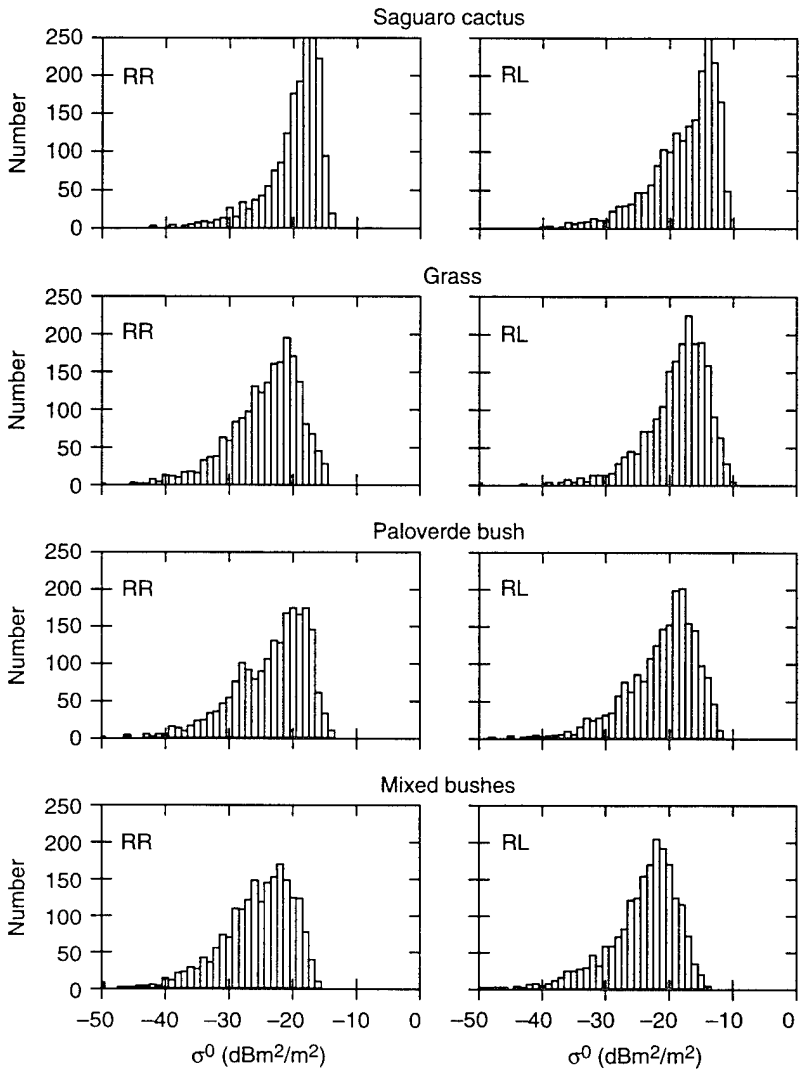

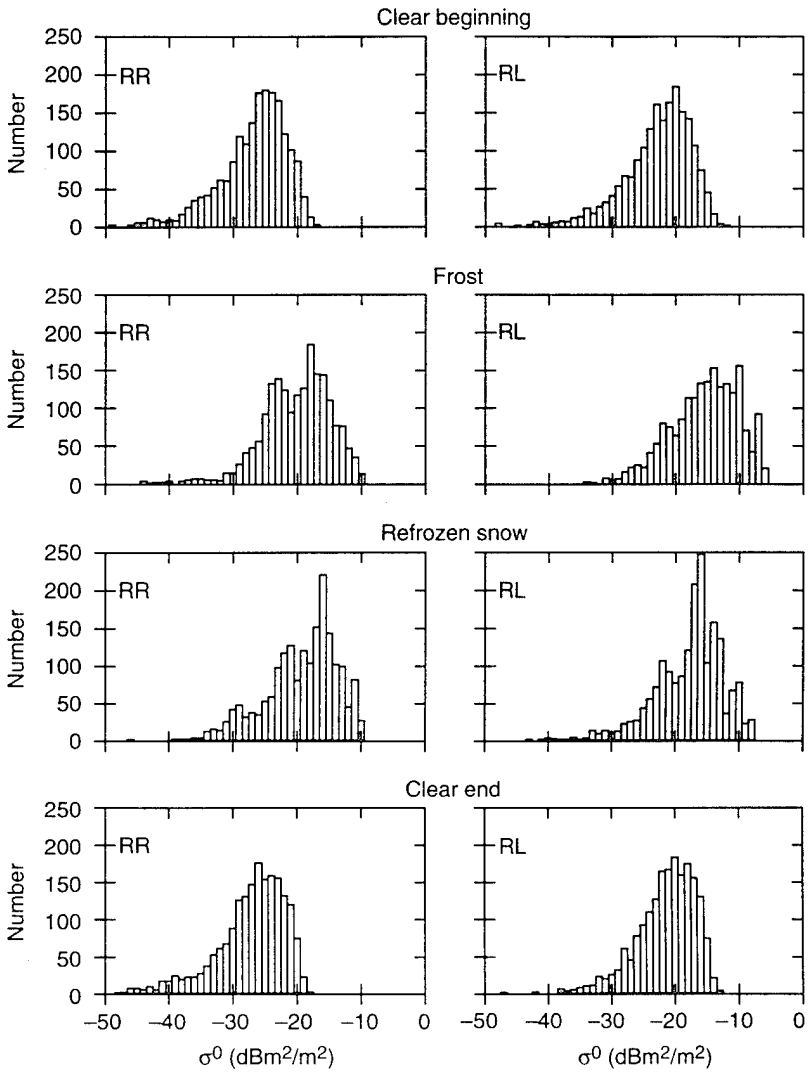


**Figure 19. Sample histograms for dirt and grass cell from Grayling I test for RR and RL polarizations for different environmental conditions.**

The spatial distribution of the clutter is very important for determining and predicting the performance of any MMW system operating in a clutter environment. To this end, spatial distributions have been calculated for both the Yuma and Grayling II field tests at both 15- and 1-m range resolutions for circular polarization. The spatial distributions for linear polarization are similar, and will not be discussed here. The cross-range resolution of the clutter cells is dependent on range, and varies from about 2 to 4 m. This means that the resolution cells area will be between 2 and 4 $m^2$ for the high-resolution case, and between 30 to 60 $m^2$ for the low-resolution case. These areas are quite different in spatial extent, but both spatial ranges are important to system operation. The low-resolution spatial distributions are more important for target detection, while high-resolution spatial distributions are more important for tracking. We calculated the spatial distributions, including both the areas viewed by the ASL and the TIPS sensors at Yuma, and the entire E1/E2 zone at Grayling. We identified the measurement areas within the radar scan pattern by overlaying the radar data on the survey data. When we made the multiple elevation measurements at the same azimuth and range, we identified the cells with the maximum RCS and included them in the final data set. We used this final set of cells, which includes one cell at each range and azimuth position within the measurement areas, for the spatial analysis. A sample low-resolution clutter map for Grayling II is shown in figure 20. For the low-resolution case, the spatial amplitude distributions were calculated by binning the RCS values in 1-dB increments, and plotting the number within each bin. Samples of the low-resolution spatial histograms for Grayling and Yuma for a clear, bare-ground condition are shown in figures 21 and 22. These distributions include all clutter types and shadowed cells. From the figures, it is apparent that the Grayling clutter has a somewhat wider distribution function than the clutter at Yuma, but the overall shape and mean of the distributions are similar. It is also apparent that, for each site, the RL and LR distributions are similar, and the RR and LL distributions are similar. The additional width of the Grayling distribution is caused by the large number of cells shadowed by the trees at Grayling that do not exist at the Yuma site.

To calculate the 1-m-resolution histograms, we first converted the data to 0.23-m resolution by performing a FFT of the frequency data for the cells within the regions that were selected for spatial analysis. For Yuma, we calculated a 64-pt FFT, while for Grayling a 128-pt FFT was needed. We converted each individual ramp to high resolution, and averaged the power in the individual FFTs to give one high-resolution FFT for each cell. We added four individual cells within this FFT together to get a 1-m-resolution (precisely, 0.94-m) FFT. We then computed a 1-m-resolution clutter map. (A sample map for Grayling II is shown in figure 23). We binned these high-range resolution images in 1-dB steps to produce spatial distributions over the same clutter area as for the low-resolution case. (These histograms are shown in figures 24 and 25.) Notice that the RL and LR distributions are similar, and that the RR and LL distributions are also similar, as in the case of the low-resolution distributions. However, a comparison of these figures shows some significant differences. For Yuma, the distributions look

almost normal on a logarithmic scale, which means the underlying distribution would be log normal. However, the Grayling distributions seem almost bimodal for RR and LL polarization, and there are increases in the amplitude of the distributions for RL and LR at the same location as the lower peak for the RR and LL. As we mentioned earlier, this is caused by the number of cells that are shadowed by the trees. In the high-resolution case, there are more shadowed cells by percentage than in the low-resolution case. Even though the distributions for Grayling and Yuma are different, the upper part of the distributions are almost identical—it is the lower sections that are different. These distributions did not change noticeably during the Yuma test, but for Grayling there were significant changes in weather that could and did affect the distributions.

To demonstrate the effects of weather changes on the 1-m-resolution distributions, four different conditions were selected for analysis. These conditions were: clear and dry (mission 150), melting snow (mission 10), fresh snow (mission 133), and refrozen snow (mission 20). The 1-m-resolution spatial amplitude distributions for these conditions for circular polarization are shown in figure 26. The figure shows that spatial distributions changed noticeably for different ground conditions. The distributions for RR polarization are more variable than those for RL polarization. The distribution function for RR is almost identical to the distribution for RL polarization for both the refrozen- and fresh-snow conditions, the only difference being a slight shift in the mean. This is not the case for the clear and melting-snow condition, where the distributions have the largest difference between polarizations. The overall polarization ratio RL/RR for the clutter distributions is the lowest for refrozen snow, somewhat bigger for fresh snow, larger still for clear and dry, and the largest for the melting-snow condition. It is also clear that one distribution function will not describe the 1-m spatial distributions for all environmental conditions. A more detailed analysis is required to best characterize both the 15- and 1-m distributions. This analysis will be completed in the future.

Figure 20. Sample low-resolution RCS maps for RR and RL polarization for Grayling II.

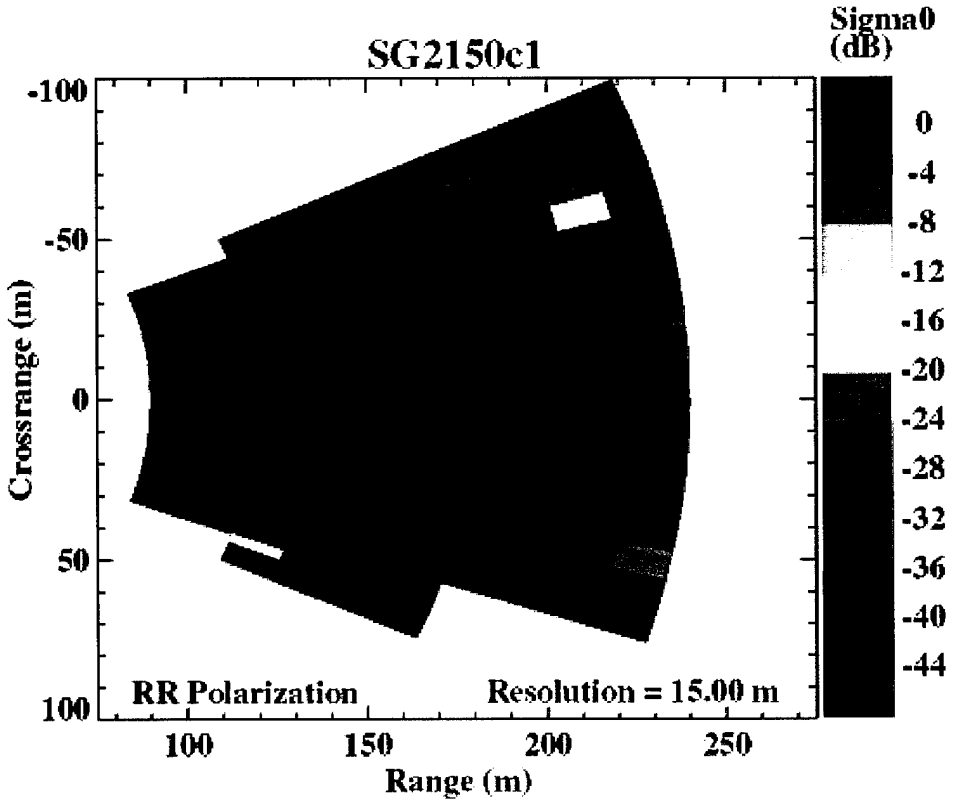


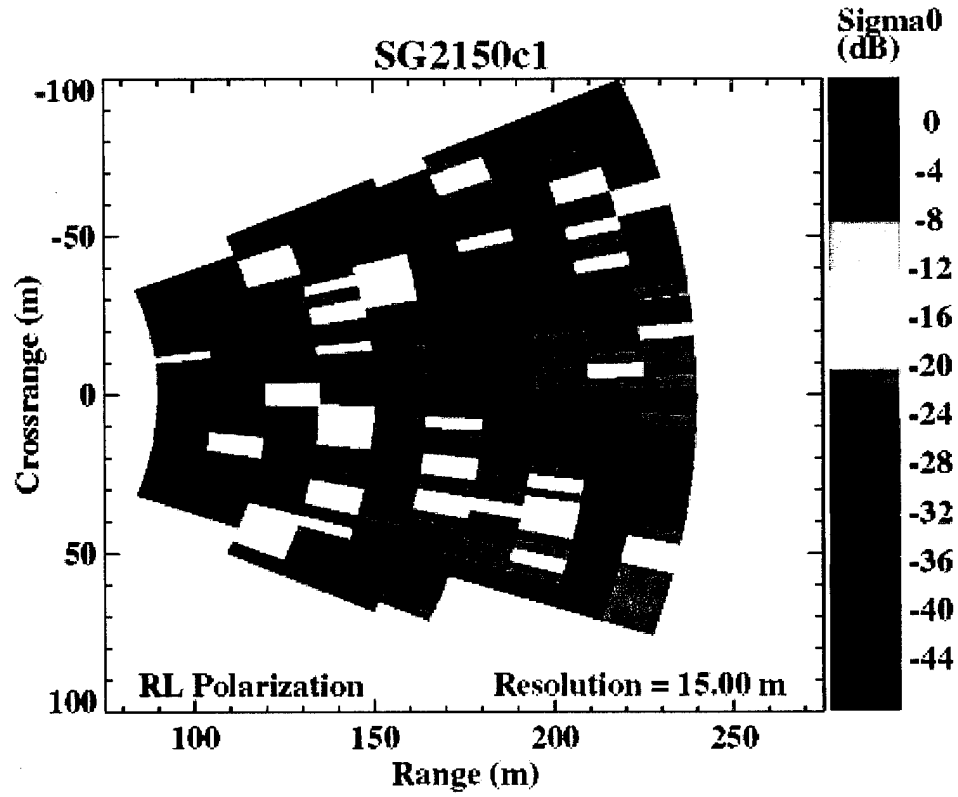

Figure 21. Sample low-resolution spatial histograms for Grayling II clutter.

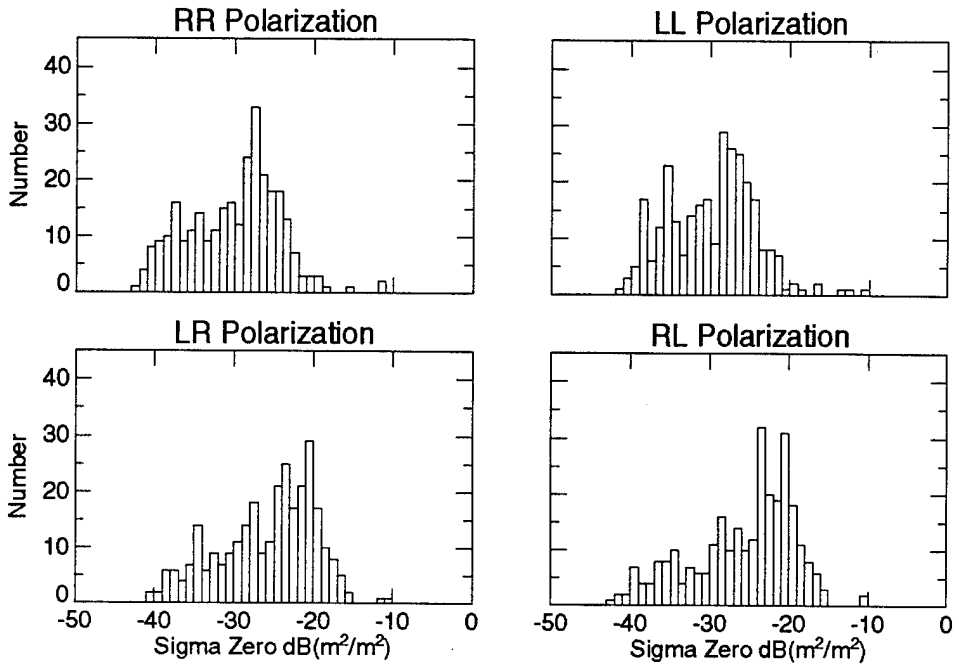


Figure 22. Sample low-resolution spatial histograms for Yuma clutter.

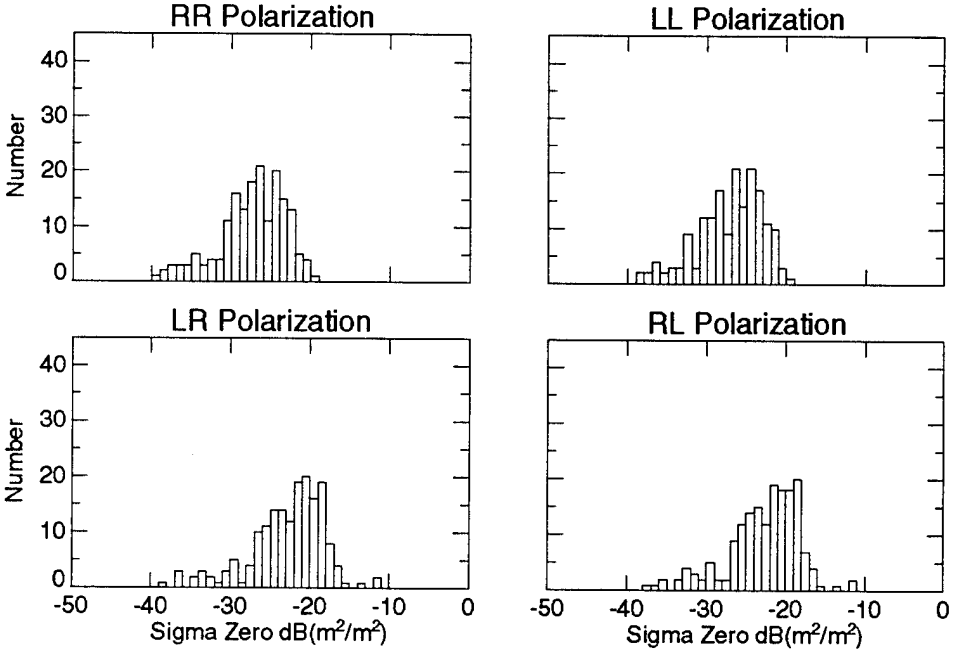

Figure 23. Sample high-range resolution RCS maps for RR and RL polarization for Grayling II.

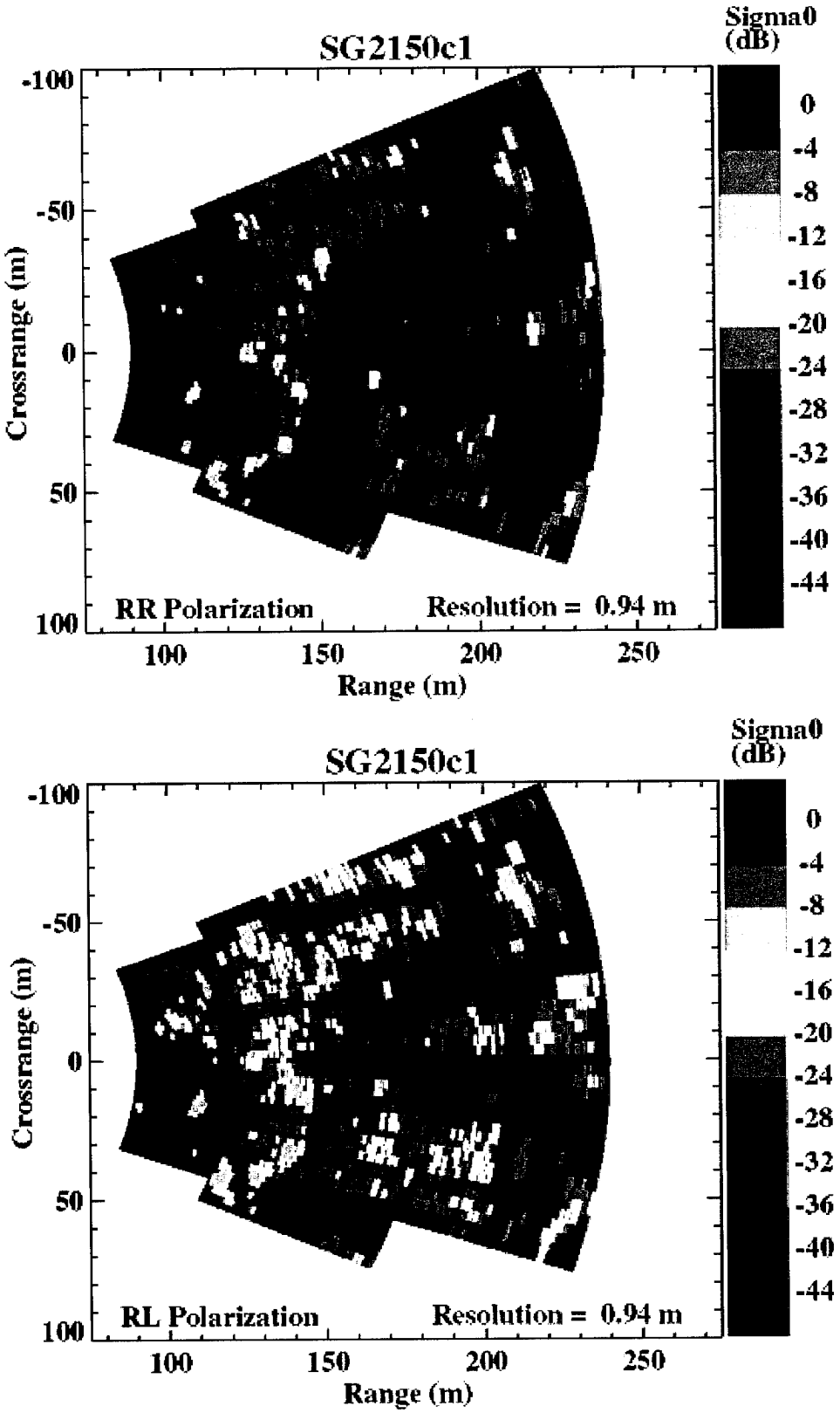

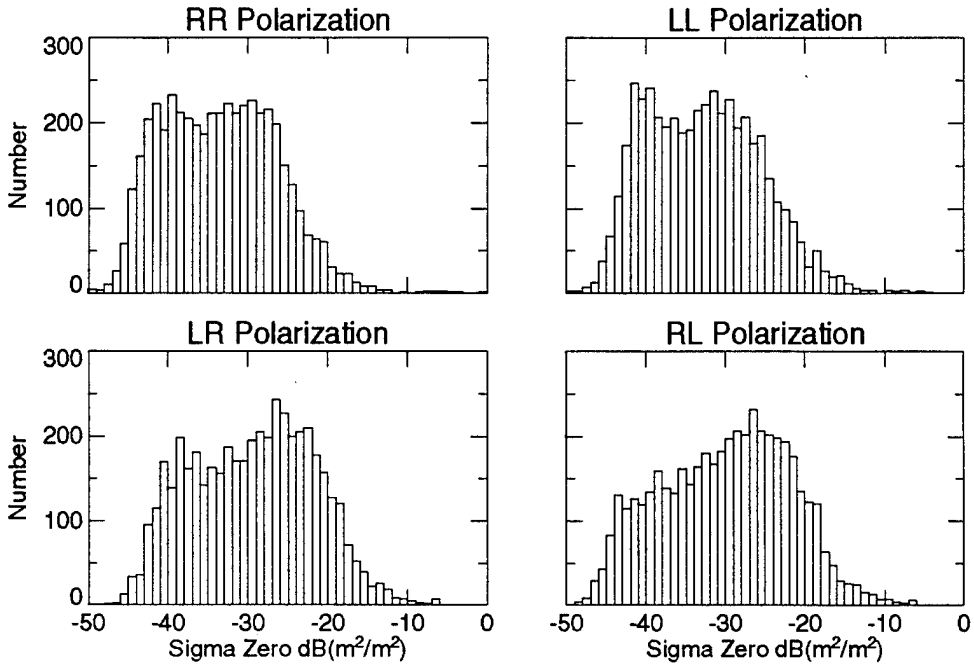


**Figure 24. Sample high-resolution spatial histograms for Grayling II clutter.**

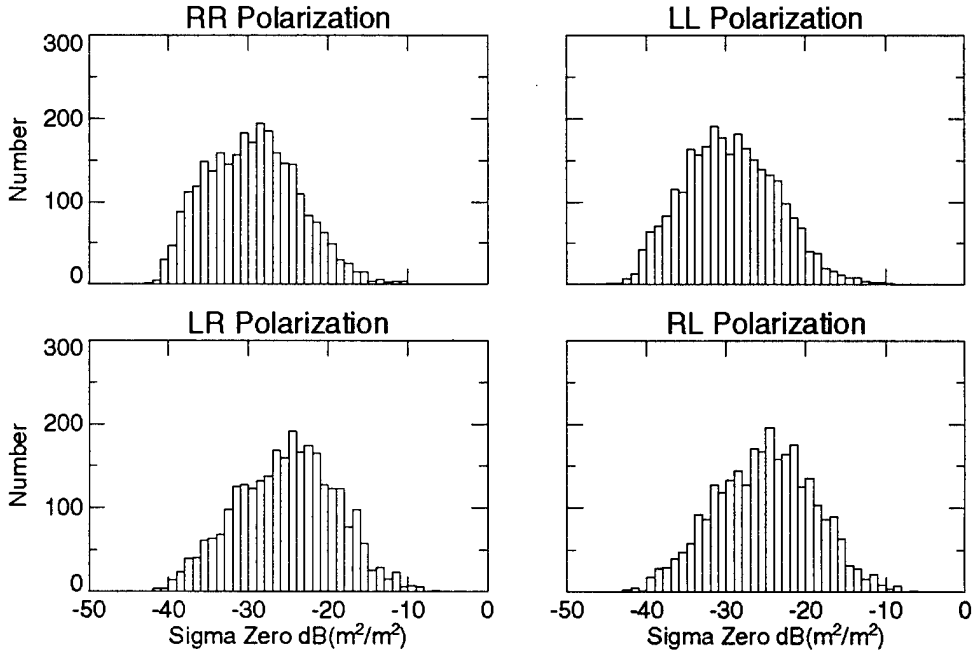


**Figure 25. Sample high-resolution spatial histograms for Yuma clutter.**

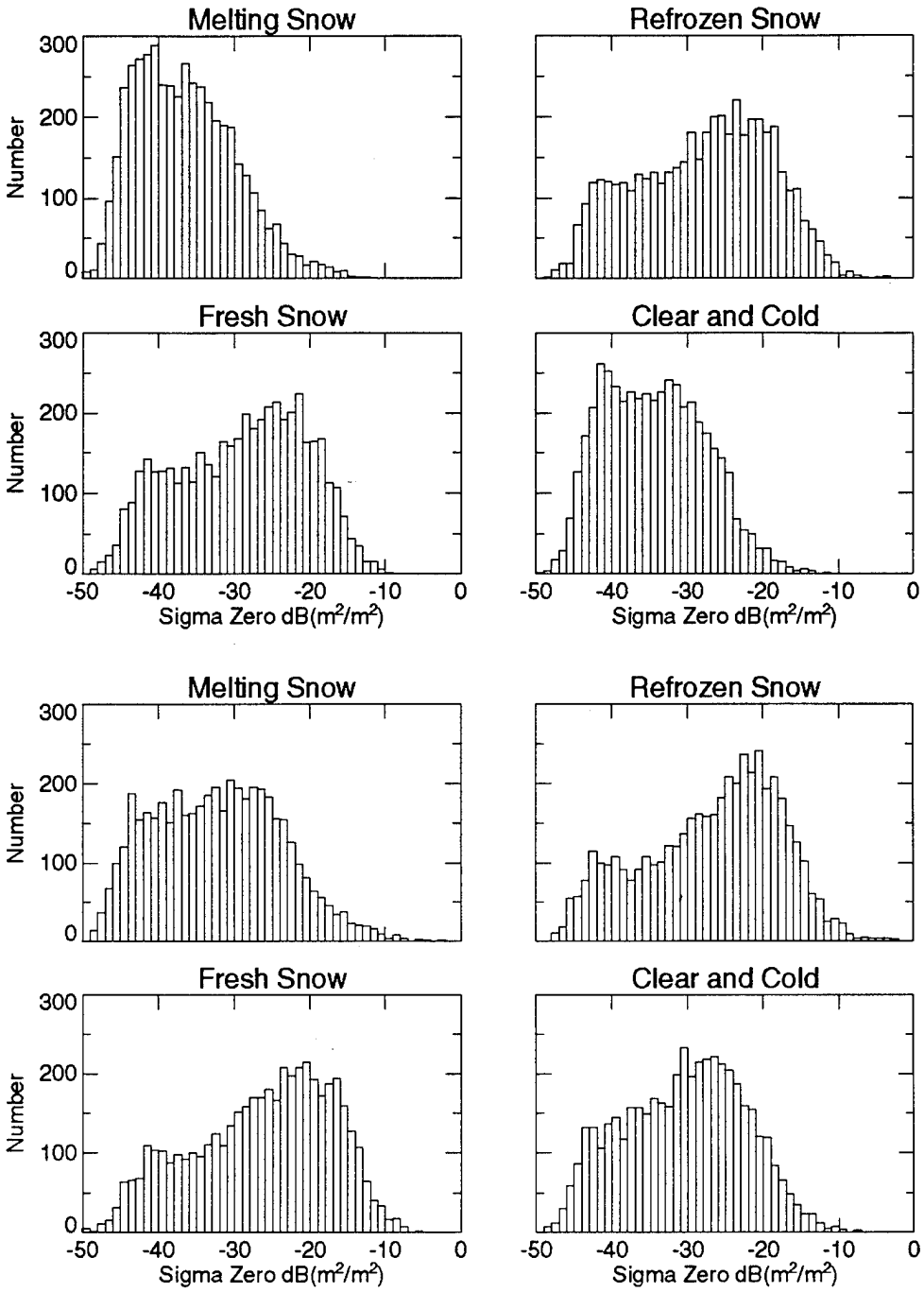


**Figure 26. Sample high-resolution spatial histograms for RR polarization above and RL polarization below for Grayling II for different ground conditions.**

# 4. Empirical Modeling

## 4.1 Modeling Procedures

Since we described the radar in section 2, only specifications relevant to the modeling effort will be repeated in this discussion. We limited the modeling effort to circular polarization because of the limited amount of linear data available for the Yuma test. The radar pulse width was 100 ns, which corresponds to a clutter cell length of 15 m. The antenna had a two-way beamwidth of approximately 1.0°, which corresponds to a clutter cell width of approximately 2.6 m at a range of 150 m. The signal-to-noise ratio was approximately 20 to 30 dB.

We collected the ARL data sets analyzed over an approximately 6- to-7-week period in the late spring of 1993 at Yuma, and in the early spring of 1994 at Grayling. The Grayling location is similar to a European environment, and the Yuma location is a desert environment. We collected data at two rectangular sites at the Yuma location, one approximately 30 by 60 m, and the other about 60 by 60 m, at a range of approximately 100 to 180 m from the radar. We collected data at one site approximately 100 by 100 m at Grayling, at a range beginning at 100 m from the radar, and ending at about 200 m from the radar. The radar depression angles were between 2° and 5°.

We scanned the designated sites at two or three different radar depression angles (the angle incremented by 1° after each azimuth scan), selecting the scan patterns to maximize the amount of ground-clutter data collected at each site, while minimizing the acquisition time. We analyzed the data with frequency-averaged $\sigma^0$ values. We selected clutter cells for analysis by measuring the radar at each range and azimuth position that yielded the highest average $\sigma^0$ among the different elevation angles, assigning each clutter cell a specific vegetation type by examining an overlay of the vegetation survey data provided by Waterways Experiment Station (WES) on high-range-resolution clutter maps. A breakdown for the cell types, number of cells of each type, and descriptions of the vegetation types determined for the ground clutter cells at Yuma and Grayling is given in tables 6 and 7.

For the Grayling site, the tree vegetation types were described as "large" or "small." This descriptor was based upon the relative RCS contribution of the trees in a clutter cell, compared to the RCS of the surrounding grass and dirt and not upon the absolute magnitude of $\sigma^0$. A difference of approximately 10 dB or greater was considered large. More coniferous trees were classified as large, compared to deciduous trees, because the deciduous trees had no leaves during the test and, therefore, usually had a smaller RCS. We did not analyze small coniferous vegetation or small mixed vegetation because of the few clutter cells with those classifications.

We divided the tests into approximately three missions per day (1-hour measurement intervals selected at random) during the data-collection periods; within each mission we made several radar scans of the entire designated areas. For the Yuma data set, we usually made two or three data runs

**Table 6. Description of Yuma, AZ, vegetation types.**

| Vegetation type | Description | Number of cells |
|---|---|---|
| Trees | palo verde trees, large creosote bushes, and/or cactus | 48 |
| Mixed | trees and bushes with grass, dirt, and gravel | 12 |
| Shadowed | low-lying or shadowed vegetation | 79 |

**Table 7. Description of Grayling, MI, vegetation types.**

| Vegetation type | Description | Number of cells |
|---|---|---|
| Grass | grass and dirt with an occasional small bush | 103 |
| Large deciduous | large deciduous trees | 10 |
| Small deciduous | small deciduous trees with grass and dirt | 20 |
| Large coniferous | large coniferous trees | 22 |
| Small coniferous | small coniferous trees with grass and dirt | 1 |
| Large mixed | large and small coniferous and deciduous trees | 8 |
| Small mixed | small coniferous and deciduous trees with grass, bushes, and dirt | 2 |
| Shadowed | low-lying or shadowed vegetation | 126 |

with circular polarization for each mission. These intra-mission data were determined to be highly correlated and, therefore, were averaged. For the Yuma test, we used data from a total of 80 missions for the analysis. For the Grayling data set, we usually made two data runs with circular polarization for each mission. Because of the changing environmental conditions during the missions, the intra-mission data were not highly correlated and, therefore, we did not average them. For the Grayling test, we used data for a total of 253 runs for analysis.

## 4.2 Analysis

We developed a multivariate linear regressive model that described the long-term trends in $\sigma^0$ for different vegetation types and polarizations. We analyzed the data by averaging the $\sigma^0$ values together (in $dBm^2/m^2$) for each vegetation type and polarization for each mission for the Yuma data set, and for each run within a mission for the Grayling data set. We examined the effects of all the relevant measured direct and indirect environmental parameters on the average value of $\sigma^0$ for each vegetation type and polarization. We considered the following parameters to be independent variables for the Yuma $\sigma^0$ model: chronological time, time of day relative to sunrise, relative humidity, absolute humidity, temperature, solar flux, wind speed, and average soil moisture content. We measured relative humidity, temperature, solar flux, and wind speed every hour, and soil moisture content once per day at several locations. For the Grayling $\sigma^0$

model, we considered the following additional parameters: snow cover, water cover, snow depth, snow density, snow grain diameter, and the equivalent water content of the snow. We usually measured these parameters once per day, and also examined interactions between selected parameters. We did not include chronological time in the Grayling $\sigma^0$ model, because we surmised that it was an indirect variable that could be expressed through other more direct variables. We examined all the parameters described above as possible independent variables for the model by visual inspections of the plots of the averaged $\sigma^0$ values versus selected parameters, and by analyzing the F values and correlation coefficients obtained from various least-square-fit analyses of the data.

Initially, we performed the model calculations separately on $\sigma^0$ values measured with RL, LR, RR, and LL polarization. The results indicated that the cross-polarization (RL and LR) and the co-polarization (RR and LL) results were within the expected error rate. Although a paired-t test indicated that neither the co- nor cross-polarization measurements were equal, the differences were usually very small (less than 0.3 dB). This result justified averaging together the co-polarization $\sigma^0$ measured values and averaging together the cross-polarization $\sigma^0$ measured values before calculating the model.

### 4.2.1 *Yuma Data*

Our analysis of the data collected at Yuma indicated that chronological time was the most significant parameter, and that soil moisture content and relative humidity were the next most significant parameters. The average $\sigma^0$ values measured for different vegetation types and polarizations at Yuma were modeled by

$$\sigma^0_{ij} = \beta_{0ij} + \beta_{1ij} T_m + \beta_{2ij} M_m + \beta_{3ij} R_m + \varepsilon_{ij}, \qquad (1)$$

where $\sigma^0$ is in $dBm^2/m^2$, $i$ = vegetation type, $j$ = co- or cross-circular-polarization, $\beta$ = model coefficients, $T$ = chronological time in hours/10000, $M$ = soil moisture content in percent/100, $R$ = relative humidity in percent/100, $m$ = index of the corresponding variable associated with a particular mission number, and $\varepsilon$ = randomly distributed error with zero mean and a standard deviation in dB. Figures 27 and 28 show a plot of the measured $\sigma^0$ values and the fit resulting from applying equation (1) with the coefficients listed in table 8. The symbols show the measured data points and the lines show the model calculations. The residue of the modeled minus the measured $\sigma^0$ values was approximately normally distributed.

The model coefficients and their standard error rates for different polarization and vegetation types are shown in table 8. You can determine the significance of the coefficients by multiplying the coefficients by the range of the corresponding independent variables. The chronological time varied from the start of the measurements on 15 March to the end of the measurements on 30 April, or from 0 to 1100 hours. Soil moisture content varied from 0.96 to 5.18 percent, with a mean of 1.97 percent; relative humidity

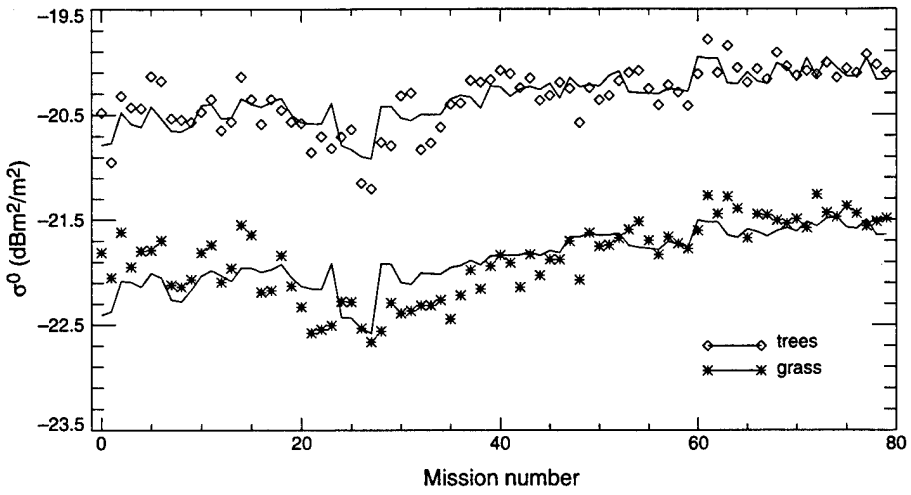


**Figure 27. Model calculations and measurements of $\sigma^0$ for tree and grass vegetation at Yuma, AZ, with circular cross-polarization.**

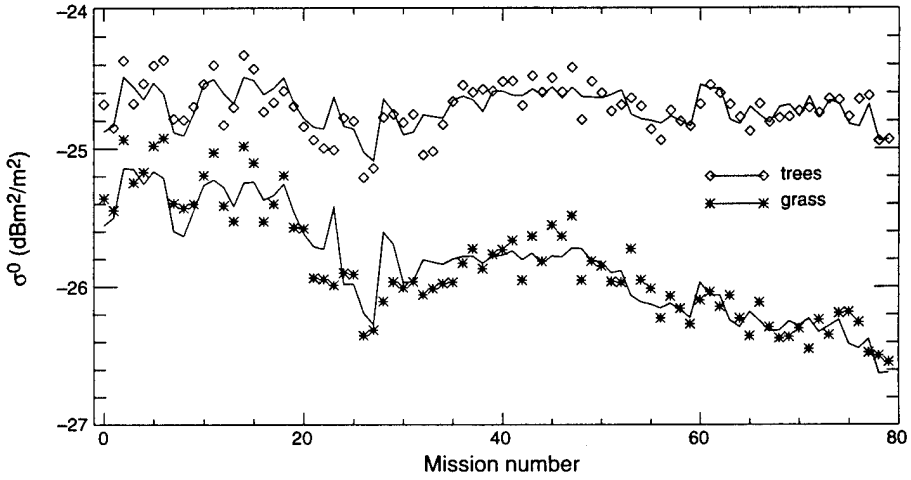


**Figure 28. Model calculations and measurements of $\sigma^0$ for tree and grass vegetation at Yuma, AZ, with circular co-polarization.**

**Table 8. Linear model coefficients calculated from Yuma $\sigma^0$ values.**

| Vegetation type | Polarization | $\sigma^0$ offset | Chronological time | Soil moisture | Relative humidity |
|---|---|---|---|---|---|
| Trees | cross | −20.16 ± 0.09 | 3.0 ± 0.7 | −11 ± 3 | −0.5 ± 0.2 |
| Grass | cross | −21.67 ± 0.12 | 3.8 ± 1.0 | 14 ± 4 | −0.5 ± 0.2 |
| Mixed | cross | −21.81 ± 0.14 | 6.7 ± 1.1 | −18 ± 4 | −0.4 ± 0.2 |
| Trees | co | −24.25 ± 0.06 | −3.1 ± 0.5 | −5 ± 2 | −0.8 ± 0.1 |
| Grass | co | −24.69 ± 0.08 | −13. ± 0.7 | −11 ± 3 | −0.9 ± 0.1 |
| Mixed | co | −24.85 ± 0.10 | −9.8 ± 0.8 | −10 ± 3 | −1.0 ± 0.2 |

varied from 2 to 74 percent, with a mean of 26 percent. The most significant change in $\sigma^0$ was a 1.5-dB decrease over chronological time for the $\sigma^0$ of grass measured with co-polarization. The effects of soil moisture content and relative humidity on $\sigma^0$ varied, but on average they were responsible for a maximum change of about 0.5 dB. The mixed vegetation coefficients showed some unexpected variations. Because mixed vegetation is a combination of tree and grass vegetation, we expected that the mixed model coefficients would fall between the grass and tree coefficients; however, this did not occur for all coefficients, due perhaps to the small sample size of the mixed vegetation type, or the fact that only small trees were included in this vegetation type (small trees may have different clutter characteristics than large trees).

The most significant environmental parameter determined by the model was chronological time, which physically appears to describe the accumulated drying effect of the sun, primarily on grass vegetation over time. This explanation is supported by the previous weather conditions. Heavy rains occurred earlier than expected at Yuma, which resulted in the peak of the desert bloom occurring before the beginning of the test. The vegetation appeared to have had limited growth, and the grass appeared to dry throughout the test. A heavy rain occurred between missions 25 and 26, but because of scheduling problems, no measurements were made until two days later. The effect of the rain was still significant, but the changes in $\sigma^0$ probably would have been larger if we had made measurements closer to the rain event. This factor could have resulted in the model attributing a larger change in $\sigma^0$ to the soil moisture content and relative humidity parameters. Only the cross-polarization coefficient for grass indicated an increase in $\sigma^0$ for an increase in soil moisture content. A possible physical explanation for this observation is that the grass absorbed the moisture faster than the other vegetation types. This event could change the transmission and reflection coefficients of the grass (rather than simply attenuate the radiation), thereby increasing single-bounce, cross-polarization scattering, while reducing multiple-bounce, co-polarization scattering.

The effectiveness of the model can be evaluated by examining the results in table 9. Column three shows the estimated standard deviation of the modeled minus measured $\sigma^0$ values in dB, and column four shows the correlation coefficient adjusted for the number of degrees of freedom calculated for measured and modeled $\sigma^0$ values. The standard deviation determines a quantitative error between modeled and measured $\sigma^0$ values, and the correlation coefficient determines how well the modeled and measured $\sigma^0$ values tracked. A low standard deviation and a high correlation indicate a good fit.

Table 9 shows that the correlation between the measured and modeled $\sigma^0$ values ranged from a high of 0.91 for co-polarization grass to a low of 0.72 for co-polarization trees. These values indicate that the major environmental parameters were identified and successfully used by the model to describe the variation in $\sigma^0$ over the duration of the measurement period. The standard deviation varied between 0.13 and 0.29 dB, which is slightly larger than the expected radar calibration error in $\sigma^0$ of 0.1 dB. This indicates that another variable may be required in the model, or that the vegetation types may need to be more accurately described. Because of the small number of errors in the model calculations and the limited number of mission sample points, we found that further analysis of the data to determine other model variables was unnecessary.

**Table 9. Agreement between modeled and measured $\sigma^0$ values for Yuma data set.**

| Vegetation type | Polarization | Standard deviation (dB) | Correlation coefficient |
|---|---|---|---|
| Trees | cross | 0.19 | 0.76 |
| Grass | cross | 0.25 | 0.73 |
| Mixed | cross | 0.29 | 0.77 |
| Trees | co | 0.12 | 0.72 |
| Grass | co | 0.17 | 0.91 |
| Mixed | co | 0.21 | 0.80 |

### 4.2.2 *Grayling Data*

We selected parameters for modeling the Grayling data set with the same methodology that was used for Yuma; however, for Grayling we applied the procedure separately to data collected over similar environmental conditions, rather than to the entire data set. We analyzed five environmental conditions: refrozen ground and snow, drying ground, melting snow, transitional snow, and fresh snow. We identified, but did not test, the following environmental conditions because of lack of sufficient repeat conditions: rain, freezing rain, snow, wet snow, and water-saturated ground. We assigned each data run an environmental condition determined by a qualitative evaluation of the past and present environmental data. The analysis indicated that refrozen ground and snow, as well as drying ground could be empirically modeled, and that melting, transitional, and fresh snow could not be empirically modeled with the available environmental data.

The refrozen ground and snow environmental condition consisted of refrozen snow (which was often present during the beginning of the test), frozen or frost-covered ground (which was often present during the end of the test), and a mixture of ground and snow conditions (which often occurred during the middle of the test). The air temperature was usually below 0°C. The drying-ground condition occurred primarily during the middle and end of the test; the air temperature was usually above 0°C. Drying ground could, potentially, have some snow cover, but not a large amount. A soil moisture measurement was usually performed once a day for drying ground.

Our analysis of the Grayling data set during conditions of refrozen ground and snow indicated that the most significant environmental parameters were snow cover and air temperature. For drying-ground conditions, the most significant parameters were snow cover, soil moisture content, absolute humidity, and wind speed. We measured these variables directly (except for snow cover, which we determined by examining snow maps generated by WES). We computed the snow cover ratio by calculating the ratio of the area covered by snow to the total area of the site; this calculation was often interpolated between measurements. We evaluated the model with several permutations of the snow-cover parameter: snow-cover ratio, log of the snow-cover ratio, and square root of the snow-cover ratio. The square root of the snow-cover ratio parameter consistently had the best results. The $\sigma^0$ values measured during the refrozen-ground and snow condition were modeled by

$$\sigma_{ij}^0 = \beta_{0ij} + \beta_{1ij} S_r + \beta_{2ij} t_r + \varepsilon_{ij}, \tag{2}$$

where $\sigma^0$ is in $dBm^2/m^2$, $i$ = vegetation type, $j$ = co- or cross-circular-polarization, $\beta$ = model coefficients, $S$ = square root of the snow cover-ratio in $(m^2/m^2)$, $t$ = temperature in °C, $r$ = index of corresponding variable associated with a particular data run number, and $\varepsilon$ = randomly distributed error with zero mean and a standard deviation in dB. The $\sigma^0$ values measured during the drying-ground condition were modeled by

$$\sigma_{ij}^0 = \beta_{0ij} + \beta_{1ij} S_r + \beta_{2ij} A_r + \beta_{3ij} M_r + \beta_{4ij} W_r + \varepsilon_{ij}, \tag{3}$$

where $A$ = absolute humidity in g/m$^3$, $M$ = soil moisture content in percent/100, and $W$ = wind speed in m/s. Figures 29 to 34 show the averaged $\sigma^0$ values and the fit resulting from applying equations (2) and (3) with the coefficients listed in tables 10 and 11.

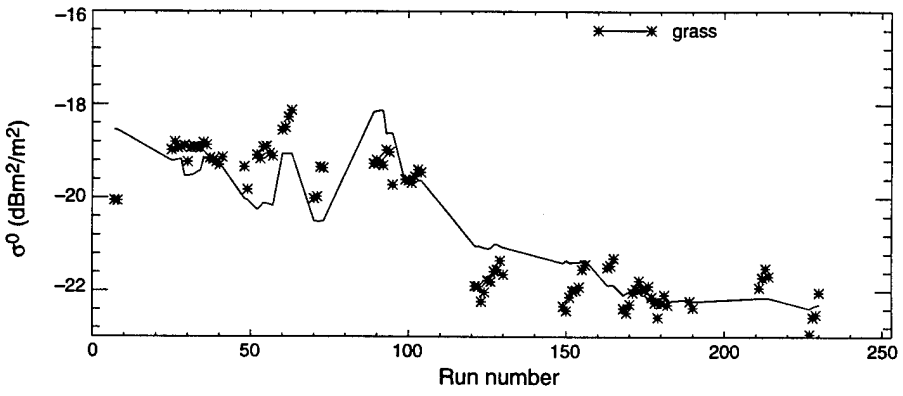


**Figure 29. Model calculations and measurements of $\sigma^0$ for grass at Grayling, MI, with circular cross-polarization for the refrozen-ground and snow condition.**

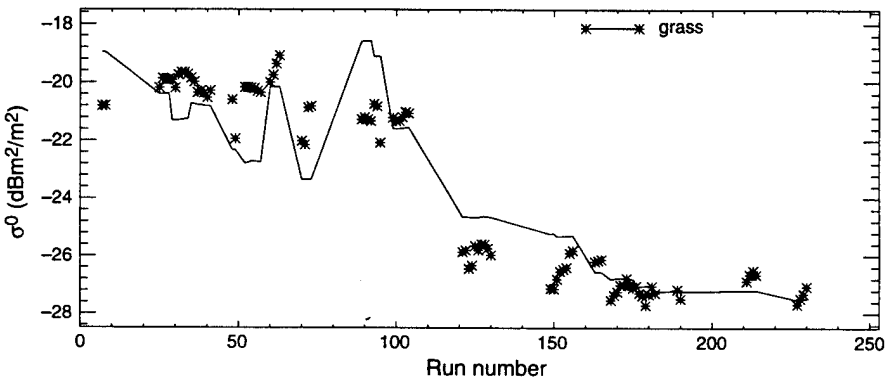


**Figure 30. Model calculations and measurements of $\sigma^0$ for grass at Grayling, MI, with circular co-polarization for the refrozen-ground and snow condition.**

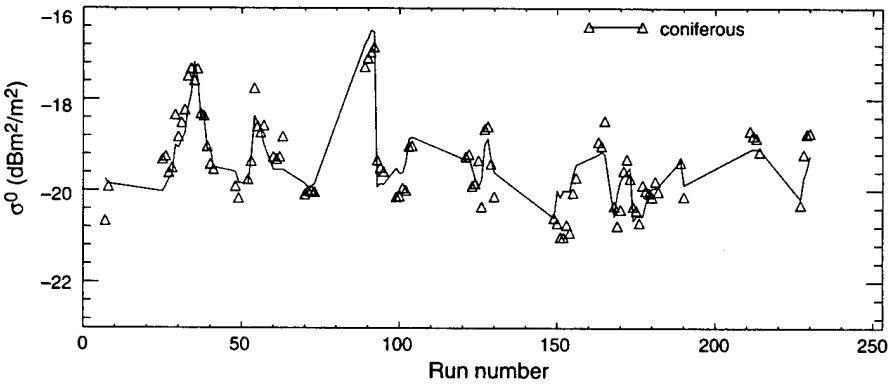


**Figure 31. Model calculations and measurements of $\sigma^0$ for coniferous trees at Grayling, MI, with circular cross-polarization for the refrozen-ground and snow condition.**

Figure 32. Model calculations and measurements of $\sigma^0$ for coniferous trees at Grayling, MI, with circular co-polarization for the refrozen-ground and snow condition.

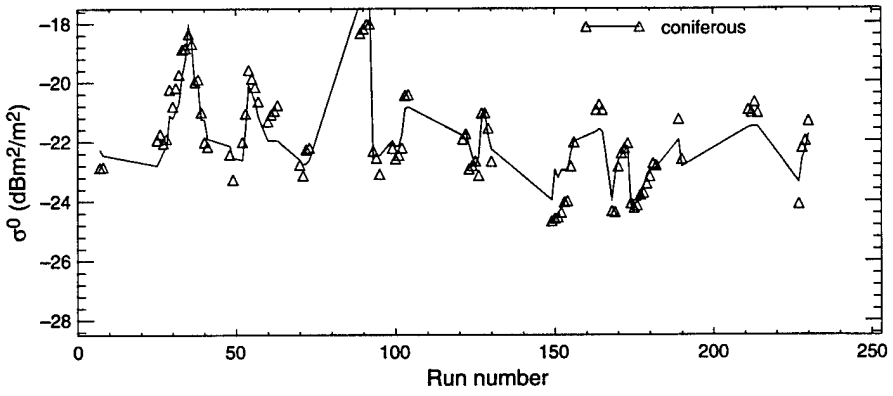


Figure 33. Model calcuations and measurements of $\sigma^0$ for coniferous trees at Grayling, MI, with circular cross-polarization for the drying-ground condition.

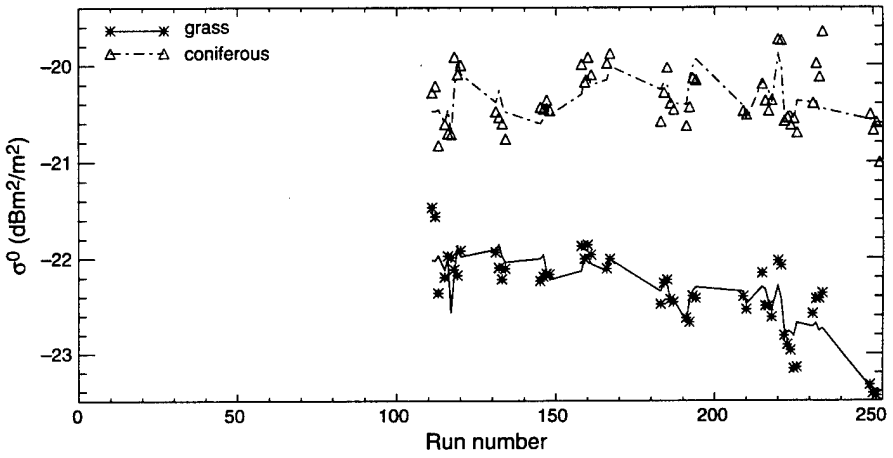


Figure 34. Model calcuations and measurements of $\sigma^0$ for coniferous trees at Grayling, MI, with circular co-polarization for the drying-ground condition.

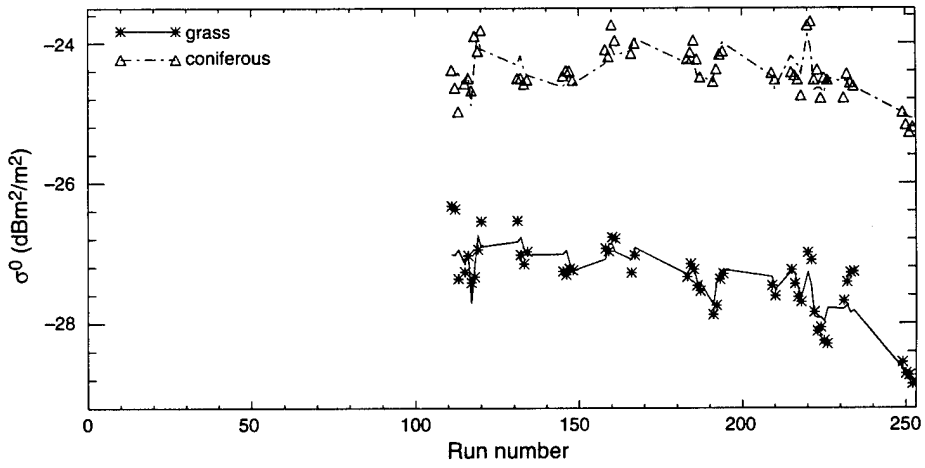

The model coefficients and their standard errors for refrozen ground and snow and for drying ground are shown in tables 10 and 11. The significance of the linear coefficients on $\sigma^0$ can be determined by multiplying the coefficients by the range of the corresponding independent variables. We analyzed data runs from 4 March to 14 April. During the refrozen-ground condition, the temperature varied from –18.4 to 0.2°C, with an average temperature of –5.5°C. The square root of the snow-cover ratio varied from 0.0 to 1.00, with an average of 0.45. During the drying-ground condition, the soil moisture varied from 4.6 to 43.3 percent (averaging 22.6 percent); absolute humidity varied from 1.7 to 6.1 g/m$^3$ (averaging 3.4 g/m$^3$); the square root of the snow-cover ratio varied from 0.0 to 0.45 (averaging 0.13); and the wind speed varied from 1.0 to 5.4 m/s (averaging 2.6 m/s).

The results for the model during the refrozen-ground and snow condition indicate that, for co-polarization, the $\sigma^0$ value of coniferous trees was mainly dependent on the temperature; the $\sigma^0$ value of grass was mainly dependent on the snow cover; and the $\sigma^0$ values for the remaining vegetation types were dependent on a combination of both parameters. The model calculation of $\sigma^0$ for coniferous trees for co-polarization changed by 5.8 dB over the temperature range, and the model calculation of $\sigma^0$ for grass for co-polarization changed by 8.8 dB over the snow-cover range. The cross-polarization calculations showed a similar trend, but with smaller changes in $\sigma^0$. The results for the drying-ground condition indicate that the co- and cross-polarization results for all vegetation types were

**Table 10. Linear model coefficients calculated for the refrozen-ground and snow condition.**

| Vegetation type | Polarization | $\sigma^0$ offset | Temperature | Snow cover |
|---|---|---|---|---|
| Grass | cross | –22.44 ± 0.14 | –0.02 ± 0.02 | 4.0 ± 0.2 |
| Deciduous large | cross | –21.56 ± 0.10 | –0.03 ± 0.01 | 1.5 ± 0.1 |
| Deciduous small | cross | –22.35 ± 0.11 | –0.01 ± 0.01 | 2.9 ± 0.2 |
| Coniferous large | cross | –20.81 ± 0.09 | –0.18 ± 0.01 | 0.9 ± 0.1 |
| Mixed large | cross | –18.98 ± 0.09 | –0.09 ± 0.01 | 1.2 ± 0.1 |
| Grass | co | –27.55 ± 0.28 | –0.01 ± 0.03 | 8.8 ± 0.4 |
| Deciduous large | co | –27.77 ± 0.16 | –0.07 ± 0.02 | 4.2 ± 0.2 |
| Deciduous small | co | –27.76 ± 0.24 | –0.02 ± 0.03 | 7.2 ± 0.4 |
| Coniferous large | co | –24.42 ± 0.14 | –0.31 ± 0.02 | 2.0 ± 0.2 |
| Mixed large | co | –23.67 ± 0.13 | –0.19 ± 0.02 | 2.9 ± 0.2 |

**Table 11. Linear model coefficients calculated for the drying-ground condition.**

| Vegetation type | Polarization | $\sigma^0$ offset | Soil moisture | Absolute humidity | Snow cover | Wind speed |
|---|---|---|---|---|---|---|
| Grass | cross | –22.20 ± 0.14 | –1.0 ± 0.4 | –0.17 ± 0.03 | 1.9 ± 0.2 | 0.14 ± 0.03 |
| Deciduous large | cross | –20.87 ± 0.18 | –0.4 ± 0.5 | –0.12 ± 0.06 | 0.5 ± 0.3 | 0.01 ± 0.04 |
| Deciduous small | cross | –22.11 ± 0.15 | –1.5 ± 0.4 | –0.15 ± 0.03 | 1.0 ± 0.2 | 0.13 ± 0.03 |
| Coniferous large | cross | –20.54 ± 0.15 | –0.2 ± 0.4 | –0.06 ± 0.02 | –0.5 ± 0.2 | 0.19 ± 0.03 |
| Mixed large | cross | –18.89 ± 0.20 | +0.5 ± 0.5 | –0.13 ± 0.05 | 0.4 ± 0.3 | 0.10 ± 0.05 |
| Grass | co | –27.13 ± 0.17 | –1.1 ± 0.4 | –0.24 ± 0.04 | 2.1 ± 0.3 | 0.20 ± 0.04 |
| Deciduous large | co | –27.33 ± 0.15 | –0.6 ± 0.4 | –0.20 ± 0.03 | 1.0 ± 0.2 | 0.05 ± 0.03 |
| Deciduous small | co | –27.80 ± 0.25 | –1.2 ± 0.6 | –0.19 ± 0.06 | 1.5 ± 0.4 | 0.20 ± 0.06 |
| Coniferous large | co | –24.45 ± 0.13 | –0.8 ± 0.3 | –0.12 ± 0.03 | –0.0 ± 0.2 | 0.24 ± 0.03 |
| Mixed large | co | –23.74 ± 0.24 | –0.5 ± 0.6 | –0.23 ± 0.06 | 0.6 ± 0.4 | 0.18 ± 0.06 |

dependent on soil moisture, absolute humidity, snow cover, and wind speed, with no one dominant parameter. These variables were responsible for a maximum deviation in $\sigma^0$ of 1.1 dB, and were often responsible for a maximum deviation in $\sigma^0$ of 0.5 dB or less. $\sigma^0$ values were usually reduced when the parameters soil moisture, absolute humidity, and wind speed indicated a reduction in the amount of water in the ground clutter.

The effectiveness of the model can be evaluated by examining the correlation coefficients and the standard deviation results shown in tables 12 and 13. These tables have the same format as the tables given in the discussion of the Yuma results. The refrozen-ground and snow condition results shown in table 12 indicate that the modeled and measured $\sigma^0$ values had either a high correlation or a small standard deviation, but not both. The lowest correlation was 0.75 for large deciduous trees measured with cross-polarization, along with a corresponding good standard deviation of 0.46 dB. The highest correlation values were over 0.90, but usually had standard deviations over 1.0 dB. These results indicate that another variable may be required in the model. The standard deviation results were much better for the drying-ground model results in table 13, but the correlation values were slightly lower. Overall, the grass and coniferous tree vegetation had better model results than deciduous tree vegetation.

**Table 12. Agreement between modeled and measured $\sigma^0$ values for refrozen-ground and snow condition.**

| Vegetation type | Polarization | Standard deviation (dB) | Correlation coefficient |
|---|---|---|---|
| Grass | cross | 0.65 | 0.89 |
| Deciduous large | cross | 0.46 | 0.75 |
| Deciduous small | cross | 0.54 | 0.87 |
| Coniferous large | cross | 0.44 | 0.89 |
| Mixed large | cross | 0.42 | 0.81 |
| Grass | co | 1.32 | 0.91 |
| Deciduous large | co | 0.75 | 0.89 |
| Deciduous small | co | 1.10 | 0.91 |
| Coniferous large | co | 0.64 | 0.92 |
| Mixed large | co | 0.60 | 0.91 |

**Table 13. Agreement between modeled and measured $\sigma^0$ values for the drying-ground condition.**

| Vegetation type | Polarization | Standard deviation (dB) | Correlation coefficient |
|---|---|---|---|
| Grass | cross | 0.23 | 0.87 |
| Deciduous large | cross | 0.29 | 0.45 |
| Deciduous small | cross | 0.24 | 0.80 |
| Coniferous large | cross | 0.23 | 0.64 |
| Mixed large | cross | 0.32 | 0.44 |
| Grass | co | 0.27 | 0.88 |
| Deciduous large | co | 0.24 | 0.75 |
| Deciduous small | co | 0.40 | 0.71 |
| Coniferous large | co | 0.21 | 0.81 |
| Mixed large | co | 0.39 | 0.65 |

The radar calibration error varied for different weather conditions. For warm weather conditions, the average calibration error for $\sigma^0$ was approximately 0.1 dB, and for snowing and freezing weather conditions, the calibration error was approximately 0.3 dB. Snow and ice collected in some of the calibration reflectors for several runs during the refrozen-ground and snow environmental conditions. (We took steps to minimize this effect, but it could not be entirely eliminated.) The standard deviation results for several vegetation types and polarizations were significantly larger than the radar calibration error.

The refrozen-ground and snow model results, in general, had poor quantitative agreement with the measured data relative to the expected calibration error. The high-correlation coefficients indicated that the major parameters were included in the model, but some minor parameters were not identified. We did not include snow liquid water content, snow density, and grain-size diameter in the model, because at the once-per-day sample rate, they were not statistically significant parameters. However, if these parameters were sampled more often or easily interpolated between measurements, we probably would have included them in the refrozen-ground and snow model, as well as in the models for the other environmental conditions that were unsuccessfully modeled.

The drying-ground model results had good quantitative agreement with the measured $\sigma^0$ values. The standard deviation results ranged from 0.2 to 0.4 dB for both polarizations, but the correlation coefficients were low for the large deciduous and mixed trees for the cross-polarization measurements. A possible explanation for this event is that these vegetation types were not affected as much by the environmental conditions, which focused more on characterizing the ground. We characterized the remaining vegetation types reasonably well by the model for both polarizations.

# 5. Conclusions

In this paper, we described in detail the 95-GHz clutter measurements taken on extensively instrumented clutter patches at Grayling, MI, and Yuma, AZ. We made the clutter measurements during the summer-to-fall and winter-to-spring transitions at Grayling, and the early-to-late-spring period at Yuma. The Grayling areas that we measured are similar to a European environment, and the Yuma test site is in a desert environment. During the measurement periods, we measured the same clutter area repeatedly, using a random-sampling plan, for both circular and linear polarization. The resulting database is useful for evaluating clutter statistics for the two environments, and for making the statistical comparisons necessary for evaluating the SWOE MMW clutter model.

We presented the RCS statistics for some selected clutter cells covering the entire measurement period at each field test. The cross-polarized return RCS's RL and LR for circular and VH and HV for linear polarization measured within individual clutters cells are virtually the same, while the co-polarized returns for both circular and linear polarization are very similar. The results for the cross-polarized radar returns are, therefore, in excellent agreement with scattering theory.

We showed that the measured RCS's varied greatly for different environmental conditions for the Grayling field tests. The grass-clutter cells were the most sensitive to changing environmental conditions (e.g., frost, fresh snow, refrozen snow, and melting snow), while the RCS changes for coniferous trees due to these conditions were not as significant. The RCS's for coniferous trees were found to increase noticeably when the temperature dropped below freezing. We also learned that the deciduous tree cells were less sensitive to changes in the weather while fully foliated than to changes in leaf condition. During the spring when leaves were not present, the RCS of the deciduous trees fluctuated almost as much as the RCS for the grass cells, due to changes in the environmental conditions. We found that clutter cells of the same type tracked each other very well. We discovered that the measured RCS's for Yuma clutter types varied very little over the measurement period, due partly to the lack of significant weather events during that timeframe.

We presented three different types of distribution functions for selected clutter cells for each clutter site. We computed histograms within individual cells across the radar bandwidth, and presented spatial amplitude histograms at both 15- and 1-m range resolutions. We showed that the frequency histograms were similar for all clutter types, with only slight differences in the means. (These distributions were similar to a log-normal distribution.) The spatial histograms were slightly different between the two clutter areas: the Grayling 15-m spatial histograms were slightly broader than those from Yuma. We also found that the Grayling 1-m spatial distributions were almost bimodal, whereas the Yuma 1-m spatial distributions indicated a log-normal distribution. These differences were due mainly to the larger number of shadowed cells produced by the trees

present in the Grayling clutter area. We found the distributions to be relatively stable during the Yuma test, while for Grayling there were large variations caused by weather changes. The frequency and spatial distributions for RR and LL polarization were more sensitive to the varying environmental conditions than the RL and LR distributions.

The $\sigma^0$ values of different vegetation types measured with circular polarization at Yuma in the spring of 1993 did not change very much. The most significant environmental parameter, as determined by an empirically calculated linear regressive model based upon least-squared estimation of $\sigma^0$, was chronological time. The physical significance of this parameter was interpreted as the accumulated drying effects of the sun. The model determined that soil-moisture content and relative humidity also had a small effect on $\sigma^0$. These parameters were significant in describing the effects caused by one large rain event.

The $\sigma^0$ values of different vegetation types measured with circular polarization at Grayling in the spring of 1994 were highly dependent on environmental conditions. A linear regressive model successfully described $\sigma^0$ measurements made during the environmental conditions of refrozen ground and snow, as well as drying ground; however, it was unsuccessful in describing $\sigma^0$ measurements made during the environmental conditions of melting, transitional, and fresh snow. The negative results were probably caused by the model's attempt to use important environmental parameters (e.g., snow density, grain-size diameter, and liquid-water content of the snow) that were sampled at a rate of once a day. This sample rate was too low for the model, and a linear interpolation between measurements was not reasonable. The $\sigma^0$ values measured during the refrozen-ground and snow conditions were dependent on the parameters of snow cover and air temperature, while $\sigma^0$ for grass was most dependent on snow cover, and the $\sigma^0$ value for coniferous trees was primarily dependent on temperature. The $\sigma^0$ values measured during the drying-ground condition were dependent on the parameters of snow cover, soil-moisture content, absolute humidity, and wind speed, with no one parameter having a dominant effect for any vegetation type. The differences between the measured and modeled $\sigma^0$ values were usually larger than the expected calibration errors of the radar system, but the correlation between the modeled and measured $\sigma^0$ values was usually high. This result indicates that, for the entire Yuma data set and for a large portion of the Grayling data set, environmental parameters were identified and incorporated into a linear model that described the variations in $\sigma^0$.

In conclusion, we have presented a small portion of RCS data obtained during extensive measurement periods for two clutter sites, those at Grayling, MI, and Yuma, AZ. An empirical model has been developed that successfully identifies the primary environmental parameters affecting the clutter background for both the Yuma and Grayling environments. A larger sample of cells would be useful for future analyses. Further work is needed to determine additional parameters responsible for some of the more subtle fluctuations in the RCS measurements, especially for Grayling clutter. This analysis, in combination with the extensive database collected at these field tests, will be an important tool for model validation and for analysis of MMW system performance.

# Acknowledgments

The work reported here was supported in part by the SWOE Program, U.S. Army Cold Regions Research and Engineering Laboratory. The support and efforts of Dr. J. P. Welsh, the SWOE program manager, are greatly appreciated and acknowledged. The participation, efforts, and contributions of Dave Wikner, Herb Dropkin, and Bob Dahlstrom, all from the $S^3I$ Directorate of the Army Research Laboratories, were critical to the successful completion of the measurement program.

# References

1. N. C. Currie and C. E. Brown (Editors), *Principles and Applications of Millimeter-Wave Radar*, Artech House, Norwood, MA (1987).

2. R. J. Wellman, J. Nemarich, H. Dropkin, D. R. Hutchins, J. L. Silvious, and D. A. Wikner, *Polarimetric Monopulse Radar Scattering Measurements of Targets at 95 GHz*, AGARD Conference Proceedings 501, Ottawa, Canada (May 1991).

3. R. J. Wellman, J. Nemarich, H. Dropkin, D. R. Hutchins, J. L. Silvious, and D. A. Wikner, *Comparison of MMW Radar Signatures of Soviet-Built Military Vehicles*, Proceedings, Precision Munitions Signatures and Simulators Conference, Eglin AFB, FL (May 1992).

4. N. C. Currie (Editor), *Radar Reflectivity Measurement: Techniques and Applications*, Artech House, Norwood, MA (1989).

5. R. M. Barnes (MIT Lincoln Laboratory), *Polarimetric Calibration Using In-Scene Reflectors*, MIT Lincoln Laboratory Project Report TT-65, Contract F19628-85-C-0002 (1986).

# Acronyms and Abbreviations

| | |
|---|---|
| A/D | analog-to-digital |
| ARL | Army Research Laboratory |
| ASL | Atmospheric Sciences Laboratory |
| DAS | data acquisition system |
| FFT | fast Fourier transform |
| HH | horizontal transmit, horizontal receive |
| HV | horizontal transmit, vertical receive |
| I/Q | in-phase/quadrature |
| IR | infrared |
| LHCP | left-hand circular polarization |
| LL | left-hand circular transmit, left-hand circular receive |
| LR | left-hand circular transmit, right-hand circular receive |
| MMW | millimeter wave |
| PDM | polarization distortion matrix |
| PRF | pulse repetition frequency |
| RCS | radar cross section |
| RHCP | right-hand circular polarization |
| RL | right-hand circular transmit, left-hand circular receive |
| RR | right-hand circular transmit, right-hand circular receive |
| SWOE | Smart Weapons Operability Enhancement |
| TIPS | Thermal Imaging Processing System |
| V | vertical polarization |
| H | horizontal polarization |
| VH | vertical transmit, horizontal receive |
| VV | vertical transmit, vertical receive |
| WES | Waterways Experiment Station |

# Distribution

Admnstr
Defns Techl Info Ctr
Attn DTIC-OCP
8725 John J Kingman Rd Ste 0944
FT Belvoir VA 22060-6218

Under Secy of Defns for Rsrch & Engrg
Attn Rsrch & Advncd Techlgy
Depart of Defns
Washington DC 20310

CECOM NVESD
Attn AMSEL-RD-NV-ASD M Kelley
Attn Techl Lib
Attn AMSEL-RD-NV-TISD F Petito
FT Belvoir VA 22060

Dpty Assist Scy for Rsrch & Techl
Attn SARD-TT D Chait
Attn SARD-TT F Milton Rm 3E479
Attn SARD-TT C Nash Rm 3E479
The Pentagon
Washington DC 20310-0103

Hdqtrs Dept of the Army
Attn DAMO-FDQ MAJ M McGonagle
400 Army Pentagon
Washington DC 20310-0460

US Army Armament RDE Ctr
Attn SMCAR-FSP P Kisatsky
Attn SMCAR-FSP-A1 R Collett
Attn SMCAR-FSP-A1 M Rosenbluth
Picatinny Arsenal NJ 07806-5000

US Army CECOM NVESD
Attn AMSEL-RD-NV-RSPO A Tarbell
Attn AMSEL-RD-SR-R J Borowick
Mailstop 1112
FT Monmouth NJ 07703-5000

US Army Materiel Command
Attn AMCDM Dir for Plans & Analysis
5002 Eisenhower Ave
Alexandria VA 22333-0001

US Army Missile Lab
Attn AMSMI-RD Advanced Sensors Dir
Attn AMSMI-RD Sys Simulation & Dev Dir
Attn AMSMI-RD-AS-MM G Emmons
Attn AMSMI-RD-AS-MM H Green

US Army Missile Lab (cont'd)
Attn AMSMI-RD-AS-MM M Christian
Attn AMSMI-RD-AS-MM M Mullins
Attn AMSMI-RD-AS-MM S Mobley
Attn AMSMI-RD-AS-RPR Redstone Sci Info Ctr
Attn AMSMI-RD-AS-RPT Techl Info Div
Redstone Arsenal AL 35809

US Army Rsrch Ofc
Attn B D Guenther
Attn C Church
PO Box 12211
Research Triangle Park NC 27709-2211

US Army Test & Evaluation Cmnd
Attn STEWS-TE-AF F Moreno
Attn STEWS-TE-LG S Dickerson
White Sands Missile Range NM 88002

USA CRREL
Attn G D Ashton
Attn SWOE G Koenig
Attn SWOE J P Welsh
72 Lyme Rd
Hanover NH 03755

USAE Waterways Exprmnt Sta
Attn CEWES-EE-S J Curtis
Attn CEWES-EN-C W West
3909 Halls Ferry Rd
Vicksburg MS 39180-6199

USATEC
Attn J N Rinker
Attn P Johnson
7701 Telegraph Rd
Alexandria VA 22315-3864

Nav Rsrch Lab
Attn 2600 Techl Info Div
4555 Overlook Ave SW
Washington DC 20375

Nav Surface Weapons Ctr
Attn DX-21 Library Div
Dahlgren VA 22448

Nav Weapons Ctr
Attn 38 Rsrch Dept
Attn 381 Physics Div
China Lake CA 93555

# Distribution

Eglin Air Force Base
Attn 46 TW/TSWM B Parnell
211 W Eglin Blvd Ste 128
Eglin AFB FL 32542-5000

USAF Wright Lab
Attn WL/MMGS B Sundstrum
Attn WL/MMGS R Smith
101 W. Eglin Blvd Ste 287A
Eglin AFB FL 32542-6810

Sandia Natl Lab
PO Box 5800
Albuquerque NM 87185

Georgia Institite of Technology
Georgia Tech Rsrch Inst
Attn Radar & Inrmntn Lab R McMillan
Attn Radar & Inrmntn Lab T L Lane
Atlanta GA 30332

Johns Hopkins Univ Applied Phys Lab
Attn D Dockery
Johns Hopkins Rd
Laurel MD 20723

Univ of Michigan Radiation Lab
Attn F Ulaby
Attn K Sarabandi
3228 EECS Bldg 1301 Beal Ave
Ann Arbor MI 48109-2122

VA Polytechnic Inst & State Univ
Elect Interaction Lab
Attn G S Brown
Bradley Dept of Elect Engrg
Blacksburg VA 24061-0111

DARPA
Attn TTO M McHenry
3701 N Fairfax Dr
Arlington VA 22203-1714

Eviron Rsrch Inst of MI
Attn IRIA Lib
PO Box 618
Ann Arbor MI 48107

Lockheed Martin CorpElect & Missile Div
Attn E Weatherwax
5600 Sand Lake Rd Mail Stop 450
Orlando FL 32819

MIT Lincoln Lab
Attn E Austin
Attn W Keicher
PO Box 73
Lexington MA 02173-9108

Simulation Technl
Attn A V Saylor
Attn D P Barr
PO Box 7009
Huntsville AL 35807

US Army Rsrch Lab
Attn AMSRL-P-S-E B Perlman
FT Monmouth NJ 07703-5601

US Army Rsrch Lab
Attn AMSRL-WT-WB R A McGee
Aberdeen Proving Ground MD 21005

US Army Rsrch Lab
Attn AMSRL-SE H Pollehn
10235 Burbeck Rd Ste 110
FT Belvoir VA 22060-5838

US Army Aberdeen Proving Ground
Attn AMXSY-MP
Aberdeen Proving Ground MD 21005-5066

US Army Rsrch Lab
Attn AMSRL-OP-SD-TA Mail & Records Mgmt
Attn AMSRL-OP-SD-Tl Tech Lib (3 copies)
Attn AMSRL-OP-SD-TP Tech Pub (5 copies)
Attn AMSRL-SE J M Miller
Attn AMSRL-SE-E J Pellegrino
Attn AMSRL-SE-EP Z G Sztankay
Attn AMSRL-SE-R A Sindoris
Attn AMSRL-SE-R E Burke
Attn AMSRL-SE-RI D Rodkey
Attn AMSRL-SE-RM B Bender
Attn AMSRL-SE-RM B Wallace
Attn AMSRL-SE-RM D Hutchins (5 copies)
Attn AMSRL-SE-RM D Wikner
Attn AMSRL-SE-RM G Goldman (10 copies)
Attn AMSRL-SE-RM H Dropkin
Attn AMSRL-SE-RM J Nemarich
Attn AMSRL-SE-RM J Silverstein

US Army Rsrch Lab (cont'd)
Attn AMSRL-SE-RM J Silvious
(10 copies)
Attn AMSRL-SE-RM R Dahlstrom
Attn AMSRL-SE-RM R Wellman
(20 copies)
Attn AMSRL-SE-RM S Straton
Attn AMSRL-SE-RS T Kipp
Attn AMSRL-SE-RU B Scheiner
Attn AMSRL-SE-RU J Sinchina
Adelphi MD 20783-1197